EUROPEAN ORGANIZATION FOR NUCLEAR RESEARCH

CERN-EP-2022-023
03 February 2022

First measurement of the absorption of $^{3}\overline{\mathrm{He}}$ nuclei in matter and impact on their propagation in the galaxy

ALICE Collaboration*

Abstract

Antimatter particles such as positrons and antiprotons abound in the cosmos. Much less common are light antinuclei, composed of antiprotons and antineutrons, which can be produced in our galaxy via high-energy cosmic-ray collisions with the interstellar medium or could also originate from the annihilation of the still undiscovered dark-matter particles. On Earth, the only way to produce and study antinuclei with high precision is to create them at high-energy particle accelerators like the Large Hadron Collider (LHC). Though the properties of elementary antiparticles have been studied in detail, knowledge of the interaction of light antinuclei with matter is rather limited. This work focuses on the determination of the disappearance probability of $^{3}\overline{\mathrm{He}}$ when it encounters matter particles and annihilates or disintegrates. The material of the ALICE detector at the LHC serves as a target to extract the inelastic cross section for $^{3}\overline{\mathrm{He}}$ in the momentum range of $1.17 \leq p < 10$ GeV/c. This inelastic cross section is measured for the first time and is used as an essential input to calculations of the transparency of our galaxy to the propagation of $^{3}\overline{\mathrm{He}}$ stemming from dark-matter decays and cosmic-ray interactions within the interstellar medium. A transparency of about 50% is estimated using the GALPROP program for a specific dark-matter profile and a standard set of propagation parameters. For cosmic-ray sources, the obtained transparency with the same propagation scheme varies with increasing $^{3}\overline{\mathrm{He}}$ momentum from 25% to 90%. The absolute uncertainties associated to the $^{3}\overline{\mathrm{He}}$ inelastic cross section measurements are of the order of 10%–15%. The reported results indicate that $^{3}\overline{\mathrm{He}}$ nuclei can travel long distances in the galaxy, and can be used to study cosmic-ray interactions and dark-matter decays.

*See Appendix A for the list of collaboration members

1 Introduction

There are no natural forms of antinuclei on Earth, but we know they exist because of fundamental symmetries in particle physics and their observation in interactions of high-energy cosmic rays and of accelerated beams. Light antinuclei, objects composed of antiprotons ($\overline{\mathrm{p}}$) and antineutrons ($\overline{\mathrm{n}}$), such as $\overline{\mathrm{d}}$ ($\overline{\mathrm{pn}}$), $^3\overline{\mathrm{He}}$ ($\overline{\mathrm{ppn}}$) and $^4\overline{\mathrm{He}}$ ($\overline{\mathrm{ppnn}}$), have been produced and studied at various accelerator facilities [1–17], including precision measurements of the mass difference between nuclei and antinuclei [18, 19]. The interest in the properties of such objects is manifold. From the nuclear physics perspective, the production mechanism and interactions of antinuclei can elucidate the detailed features of the strong interaction that binds nucleons into nuclei. From the astrophysical standpoint, natural sources of antinuclei may include annihilation of dark-matter particles such as weakly interacting massive particles (WIMPs) [20] and other exotic sources such as antistars [21, 22]. Dark matter (DM) constitutes about 27% of the total energy density budget within our universe [23] and is believed to accumulate throughout the galaxy due to its gravitational interaction with ordinary matter [24]. This is demonstrated by the measurement of the fine structure of the cosmic microwave background [25, 26], gravitational lensing of galaxy clusters [24] and the rotational curves of some galaxies [21]. Another possible source of antinuclei in our universe are high-energy cosmic-ray collisions with atoms in the interstellar medium.

The observation of antinuclei such as $^3\overline{\mathrm{He}}$ is one of the most promising signatures of dark-matter annihilation [20, 27–30]. The kinetic-energy distribution of antinuclei produced in dark-matter annihilation peaks at low kinetic energies (E_{kin} per nucleon $\lesssim$ 1 GeV/A) for most assumptions of dark-matter mass [20]. In contrast, for antinuclei originating from cosmic-ray interactions the spectrum peaks at much larger E_{kin} per nucleon $\simeq$ 10 GeV/A. Thus, the low-energy region is almost free of background for dark-matter searches.

To calculate the expected flux of antinuclei near Earth, one needs to know precisely the antinucleus formation and annihilation probabilities in the galaxy. The formation probability of light antinuclei (up to mass number $A = 4$) is currently studied at accelerators. By now, several models successfully describe light-antinuclei production yields [31–35]. Such models are based on either the statistical-hadronization [12, 36, 37] or coalescence approach [38, 39].

Another crucial aspect in the search of antinuclei in our galaxy is the knowledge of their disappearance probability when they encounter matter and annihilate or disintegrate. Antinuclei generated in our galaxy may travel thousands of light years [40] before reaching the Earth and being detected. The journey of antinuclei through the galaxy can be modelled by propagation codes, which incorporate the initial distribution of antinucleus sources, the interstellar gas distribution in the galaxy, the elastic scatterings, and the inelastic hadronic interactions with the interstellar medium. The antinucleus flux in the Solar System is further modulated by solar magnetic fields. During the entire journey, antinuclei can encounter matter and disappear. The disappearance probability is quantified through the inelastic cross section. It is normally studied employing particle beams of interest impinging on targets of known composition and thickness, but antinuclei beams are very challenging to obtain. Today, the LHC is the best facility to study nuclear antimatter since its high energies allow one to produce on average as many nuclei as antinuclei in proton–proton (pp) and lead–lead (Pb–Pb) collisions [12, 41]. The detector material can serve as a target and the disappearance probability can be determined experimentally [42].

This work presents the first measurement of the $^3\overline{\mathrm{He}}$ inelastic cross section $\sigma_{\mathrm{inel}}(^3\overline{\mathrm{He}})$, obtained using data from the ALICE experiment. These results are used in model calculations to assess the effect of the disappearance of antinuclei during their propagation through our galaxy. The associated uncertainties are estimated for the first time based on experimental data. The transparency of our galaxy to the propagation of $^3\overline{\mathrm{He}}$ nuclei stemming from a specific dark-matter source and from interactions of high-energy cosmic rays with the interstellar medium is determined, providing one of the necessary constraints for the study of antinuclei in space.

2 Determination of the inelastic cross section

The measurement of the inelastic cross sections under controlled conditions requires a beam with a well-defined momentum and a target whose material and its spatial distribution are well-known. Since no $^3\overline{\mathrm{He}}$ beams are available, we exploit the antimatter production at the LHC and the excellent identification and momentum determination for $^3\overline{\mathrm{He}}$ in ALICE as an equivalent setup. In our study, the ALICE detector itself serves as a target for the inelastic processes. A detailed description of the detector and its performance is available in Refs. [43, 44]. $^3\overline{\mathrm{He}}$ and $^3\mathrm{He}$ nuclei, serving as probes herein, are produced in pp and Pb–Pb collisions. At LHC high energies, $^3\overline{\mathrm{He}}$ and $^3\mathrm{He}$ are produced in same amounts on average. The exact primordial ratio can be derived from precise antiproton-to-proton measurements [41, 45] and in pp collisions at the centre-of-mass energy of $\sqrt{s} = 13$ TeV corresponds to 0.994 ± 0.045. The ALICE subdetectors that are considered as targets are the Inner Tracking System (ITS), the Time Projection Chamber (TPC) and the Transition Radiation Detector (TRD). A schematic representation of the ALICE detector is shown in panel a) of Fig. 1. The material composition of the three subdetectors is diverse. The detailed knowledge of the detector geometry and composition [46] allows one to determine the effective target material. $\sigma_{\mathrm{inel}}(^3\overline{\mathrm{He}})$ is estimated for three effective targets. The first one is constituted by the average material of the ITS+TPC systems (with averaged atomic mass and charge numbers of $\langle A \rangle =$ 17.4 and $\langle Z \rangle = 8.5$), the second one corresponds to the ITS+TPC+TRD systems ($\langle A \rangle = 31.8$ and $\langle Z \rangle =$ 14.8) [42], and the third one corresponds to the TRD system only ($\langle A \rangle = 34.7$ and $\langle Z \rangle = 16.1$). The values are obtained by weighting the contribution from different materials with their density times length crossed by particles.

Figure 1 shows a schematic representation of the analysis steps necessary to extract $\sigma_{\mathrm{inel}}(^3\overline{\mathrm{He}})$. Panel a) of Fig. 1 shows $^3\overline{\mathrm{He}}$ and $^3\mathrm{He}$ tracks crossing the ALICE detector, with the annihilation occurring for the $^3\overline{\mathrm{He}}$. The momentum p is measured via the determination of the track trajectory and curvature radius in the ALICE magnetic field ($B = 0.5$ T). $^3\overline{\mathrm{He}}$ and $^3\mathrm{He}$ are first identified when they reach the TPC by the measurement of their specific energy loss ($\mathrm{d}E/\mathrm{d}x$) in the detector gas. The excellent separation power of this measurement is shown in panel b) of Fig. 1, where the $\mathrm{d}E/\mathrm{d}x$ is presented as a function of the particle rigidity (p/z), where z denotes the charge of the particle crossing the TPC in units of the electron charge. The red dots represent all nuclei that are reconstructed in the TPC, while the green dots show the nuclei that survive up to the time-of-flight (TOF) detector where they are matched to a TOF hit. A more detailed description of the employed particle identification methods can be found in Methods.

We use two methods to evaluate $\sigma_{\mathrm{inel}}(^3\overline{\mathrm{He}})$. The first method, applied to pp data sample at $\sqrt{s} = 13$ TeV, relies on the comparison of the measured $^3\overline{\mathrm{He}}$ and $^3\mathrm{He}$ yields (antibaryon-to-baryon method). In this case, the experimental observable is constituted by the reconstructed $^3\overline{\mathrm{He}}/^3\mathrm{He}$ ratio analogously to the method used in Ref. [42] for (anti)deuterons. The inelastic process that takes place in the ITS, TPC or TRD material manifests itself by the fact that less $^3\overline{\mathrm{He}}$ than $^3\mathrm{He}$ candidates are detected, as depicted in panel c) of Fig. 1. The full circular blue symbols in this panel show the momentum-dependent $^3\overline{\mathrm{He}}/^3\mathrm{He}$ ratio measured in pp collisions as a function of the particle rigidity reconstructed at the primary vertex ($p_{\mathrm{primary}}/|z|$). The discontinuity of the $^3\overline{\mathrm{He}}/^3\mathrm{He}$ ratio observed at $p_{\mathrm{primary}}/|z| = 1$ GeV/c is due to the additional requirement of a hit in the TOF detector for momenta above this value. This ratio can also be evaluated by means of a full-scale Monte Carlo simulation of antinuclei and nuclei traversing the ALICE detector.

The measured observables are compared in each momentum interval with simulations where $\sigma_{\mathrm{inel}}(^3\overline{\mathrm{He}})$ is varied to obtain the inelastic cross sections. We performed several full-scale simulations with variations of $\sigma_{\mathrm{inel}}(^3\overline{\mathrm{He}})$ with respect to the standard parametrization implemented in the GEANT4 package [47, 48] as shown in panel c) of Fig. 1. Panel e) presents the simulated ratio as a function of $\sigma_{\mathrm{inel}}(^3\overline{\mathrm{He}})$ parametrized using the Lambert–Beer law [49]. For each momentum interval, the uncertainties of $\sigma_{\mathrm{inel}}(^3\overline{\mathrm{He}})$ are obtained by requiring an agreement at $\pm 1\sigma$ with the measured observables, where σ represents the total experimental uncertainty (statistical and systematic uncertainties added in

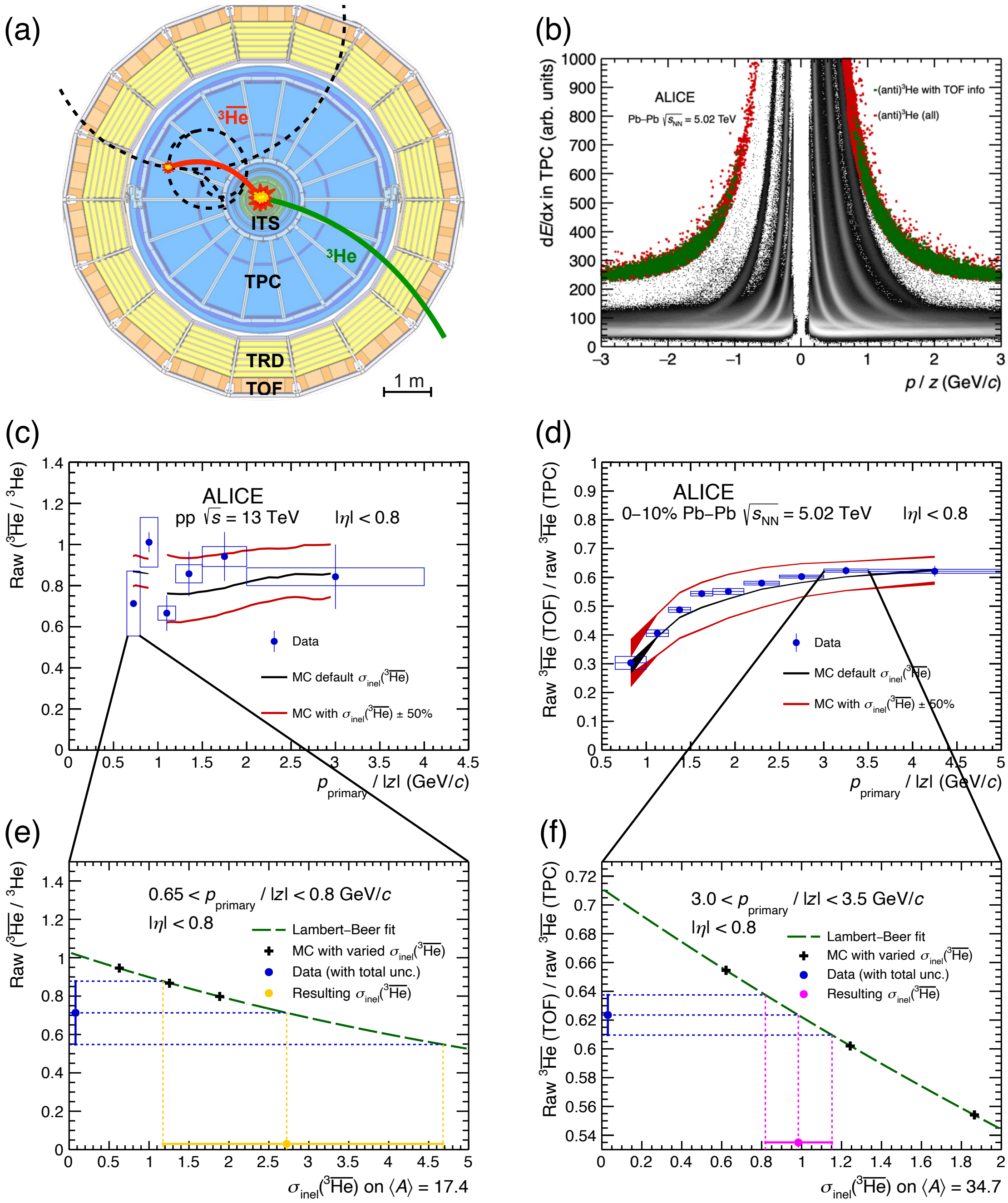

Fig. 1: Schematic representation of the inelastic processes within the ALICE detector and steps followed for the extraction of $\sigma_{\mathrm{inel}}(^{3}\overline{\mathrm{He}})$. **(a)** Representation of the ALICE detectors at midrapidity (in the plane perpendicular to the beam axis) with a $^{3}\overline{\mathrm{He}}$ undergoing annihilation in the TPC gas (in red) and a ^{3}He that does not undergo an inelastic reaction and reaches the TOF detector (in green). **(b)** Identification of (anti)nuclei by means of their specific energy loss dE/dx and momentum measurement in the TPC. The red points show all (anti)^{3}He nuclei reconstructed with the TPC detector, green points correspond to (anti)^{3}He with TOF information; other (anti)particles are shown in black. **(c)** Experimental results for the raw ratio of $^{3}\overline{\mathrm{He}}$ to ^{3}He in pp collisions at $\sqrt{s} = 13$ TeV; the black and red lines show the results from the Monte Carlo simulations with varied $\sigma_{\mathrm{inel}}(^{3}\overline{\mathrm{He}})$. **(d)** Experimental ratio of $^{3}\overline{\mathrm{He}}$ with TOF information over all reconstructed $^{3}\overline{\mathrm{He}}$ in Pb–Pb collisions at $\sqrt{s_{\mathrm{NN}}} = 5.02$ TeV. The black and red lines show the results from the Monte Carlo simulations with varied $\sigma_{\mathrm{inel}}(^{3}\overline{\mathrm{He}})$. **(e)** The raw ratio of $^{3}\overline{\mathrm{He}}$ to ^{3}He in a particular rigidity interval as a function of $\sigma_{\mathrm{inel}}(^{3}\overline{\mathrm{He}})$ for $\langle A \rangle = 17.4$. The fit shows the dependence of the observable on $\sigma_{\mathrm{inel}}(^{3}\overline{\mathrm{He}})$ according to the Lambert–Beer formula. The horizontal dashed blue lines show the central value and 1σ uncertainties for the measured observable and their intersection with the Lambert–Beer function determines $\sigma_{\mathrm{inel}}(^{3}\overline{\mathrm{He}})$ limits (orange lines). **(f)** Extraction of $\sigma_{\mathrm{inel}}(^{3}\overline{\mathrm{He}})$ for $\langle A \rangle = 34.7$ analogous to the panel **e**.

quadrature).

The second method, employed in the Pb–Pb data analysis at a centre-of-mass energy per nucleon pair $\sqrt{s_{\mathrm{NN}}} = 5.02$ TeV, measures the disappearance of $^3\overline{\mathrm{He}}$ nuclei in the TRD detector only (TOF-to-TPC method). The ratio of $^3\overline{\mathrm{He}}$ with TOF information to all $^3\overline{\mathrm{He}}$ candidates is considered as an experimental observable. Panel d) of Fig. 1 shows the momentum-dependent ratio of $^3\overline{\mathrm{He}}$ with a reconstructed TOF hit to all $^3\overline{\mathrm{He}}$ candidates extracted from Pb–Pb collisions. As with the first method, this observable is also evaluated by means of a full-scale Monte Carlo GEANT4 simulation assuming different $\sigma_{\mathrm{inel}}(^3\overline{\mathrm{He}})$. Panel f) shows the extraction of $\sigma_{\mathrm{inel}}(^3\overline{\mathrm{He}})$ and its related uncertainties for one rigidity interval following the same procedure as the one used in the first method.

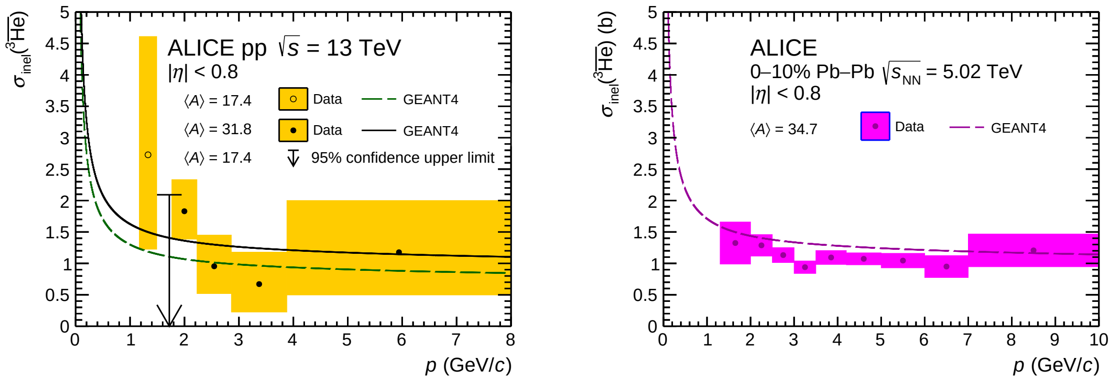

Fig. 2: Results for $\sigma_{\mathrm{inel}}(^3\overline{\mathrm{He}})$ obtained from pp collisions at $\sqrt{s} = 13$ TeV (left) and from Pb–Pb collisions at $\sqrt{s_{\mathrm{NN}}} = 5.02$ TeV (right). The dashed curves represent the GEANT4 cross sections corresponding to the effective material probed by the different analyses.

The final results are shown in Fig. 2. The left panel shows the $\sigma_{\mathrm{inel}}(^3\overline{\mathrm{He}})$ results from the pp data analysis with the yellow boxes representing the $\pm 1\sigma$ uncertainty intervals. In the right panel, the histogram with the magenta error boxes shows $\sigma_{\mathrm{inel}}(^3\overline{\mathrm{He}})$ extracted from the Pb–Pb data analysis. The results are shown as a function of the momentum p at which the inelastic interaction occurs. Due to continuous energy loss inside the detector material, this momentum is lower than p_{primary} reconstructed at the primary vertex (Methods). The copious background below $p = 1.5$ GeV/c prevents from applying the antibaryon-to-baryon ratio method in Pb–Pb collisions (Methods). Additionally, the large energy loss and bending within the magnetic field exclude the employment of the TOF-to-TPC method, since low-momentum $^3\overline{\mathrm{He}}$ tracks don't reach the TOF detector. On the other hand, for momentum values larger than $p = 1.5$ GeV/c, the yield of produced $^3\overline{\mathrm{He}}$ is substantially larger in Pb–Pb collisions, thus leading to higher statistical precision for this colliding system. The evaluation of systematic uncertainties is described in Methods. The two independent analysis methods therefore provide access to slightly different momentum ranges and to different $\langle A \rangle$ values while delivering consistent results in the common momentum region. This is the first experimental measurement of $\sigma_{\mathrm{inel}}(^3\overline{\mathrm{He}})$.

The cross section used by GEANT4 for the average mass number $\langle A \rangle$ of the material is shown by the dashed lines in Fig. 2. It is obtained from a Glauber model parametrization [48] of the collisions of $^3\overline{\mathrm{He}}$ with target nuclei in which the antinucleon–nucleon cross section value is taken from measured $\overline{\mathrm{p}}\mathrm{p}$ collisions [50]. Agreement with the experimental $\sigma_{\mathrm{inel}}(^3\overline{\mathrm{He}})$ is observed within two standard deviations in the studied momentum range.

3 Propagation of antinuclei in the interstellar medium

To estimate the transparency of our galaxy to $^3\overline{\mathrm{He}}$ nuclei, we consider two examples of $^3\overline{\mathrm{He}}$ production sources. Results of Ref. [51] are used as input for the production cross section of $^3\overline{\mathrm{He}}$ from cosmic-ray collisions with interstellar medium. As a dark-matter source of $^3\overline{\text{He}}$ we consider WIMP candidates with a mass of 100 GeV/c^2 decaying into W^+W^- pairs followed by hadronization into (anti)nuclei [27]. In both cases, the yields of produced $^3\overline{\text{He}}$ are determined employing the coalescence model that builds antinuclei from antineutrons and antiprotons that are close-by in phase space [38, 39, 52]. More details about the cosmic-ray and dark-matter sources are discussed in Methods. Additional $^3\overline{\text{He}}$ sources such as supernovae remnants [53], antistars [21, 22] and primordial black holes [54–56] have not been included in this work.

We consider the dark matter density distribution in our galaxy according to the Navarro–Frenk–White profile [57] as illustrated in the upper panel of Fig. 3 where also a schematic representation of the $^3\overline{\text{He}}$ production from cosmic-ray interaction with the interstellar gas or dark-matter annihilations is shown.

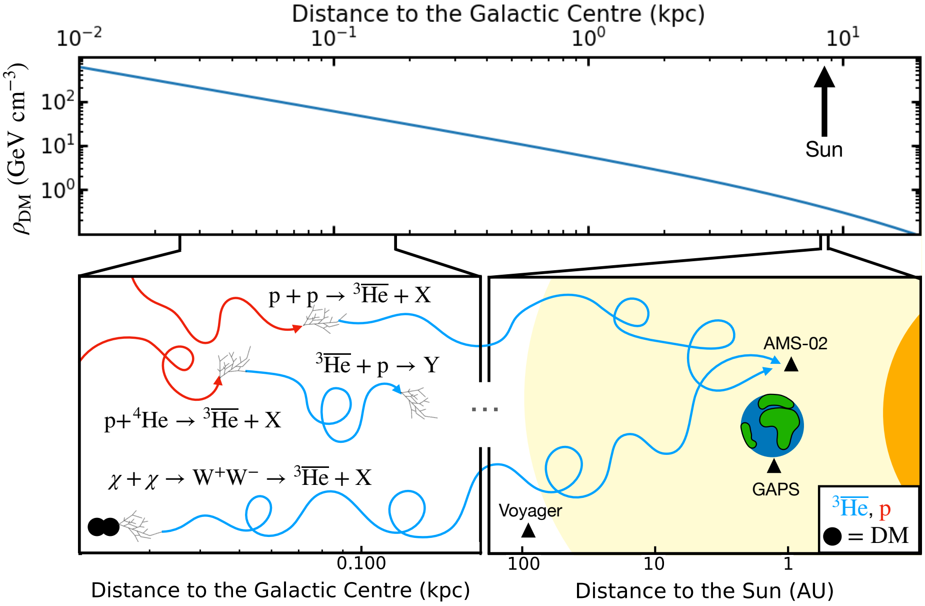

Fig. 3: (Upper Panel) Dark-matter distribution in our galaxy as a function of the distance R from the galactic centre according to the Navarro–Frenk–White profile [57]. (Lower panel) Graphical illustration of the $^3\overline{\text{He}}$ production from cosmic-ray interactions with the interstellar gas or dark-matter (χ) annihilations. The yellow halo represents the heliosphere, Earth, Sun and the positions of the Voyager 1, AMS-02 and GAPS experiments are depicted as well.

The propagation of charged particles within galaxies is driven by magnetic fields. The propagation is commonly described by a transport equation which includes the following terms: i) a source function, ii) diffusion, iii) convection, iv) momentum variations due to Coulomb scattering, diffusion and ionization processes, v) fragmentation, decays and inelastic interactions. This equation, discussed in more details in Methods, can be solved numerically employing several propagation models [58–61]. In this work the publicly available GALPROP code [1] [61] is employed. In the context of this calculation, our galaxy is approximated by a cylindrical disk filled with an interstellar gas composed of hydrogen ($\approx 90\%$) and ^{4}He ($\approx 10\%$) with an average hydrogen number density of ~ 1 atom/cm^3 [62]. The gas distribution within our galaxy is constrained by several astronomical spectroscopy measurements [63–66]. GALPROP provides the propagation of particles up to the boundaries of the Solar System. To estimate the particle flux inside the Solar System, the effect of the solar magnetic field must be taken into account. This can be achieved by employing the Force Field approximation or dedicated models like HelMod [67, 68]. The whole propagation chain is benchmarked using several species of cosmic rays, including protons and light nuclei (up to $Z = 28$) [40]. The cosmic-ray injection spectra and the propagation parameters are

[1] We use GALPROP version 56 available at https://galprop.stanford.edu.

tuned to match the measurements of protons and light nuclei both outside [69] and within the Solar System [70–72].

After their production, the $^3\overline{\text{He}}$ nuclei need to travel a distance of several kpc to reach the Earth [40, 57]. During this passage, they might encounter protons or ^{4}He nuclei in the interstellar gas and interact inelastically. To model the cross section of this process, we scale the momentum-dependent GEANT4 parametrization of the $^3\overline{\text{He}}$–p inelastic cross section with the correction factors obtained from our measurements. For the low-momentum range ($1.17 \leq p < 1.5$ GeV/c) we consider the results from pp collisions and for the high-momentum range ($1.5 \leq p < 10$ GeV/c) the results from Pb–Pb collisions. The correction factors from the ALICE measurements and their uncertainties are parametrized with a continuous function employing a combination of polynomial and exponential functions. The additional uncertainty due to scaling with A is estimated to be lower than 8% [48] (Methods). For the extrapolation to momenta above the measured momentum range, we consider the correction factor corresponding to the last measured momentum interval (Fig. 2 right). The resulting $^3\overline{\text{He}}$-p inelastic cross section as a function of the $^3\overline{\text{He}}$ kinetic energy per nucleon is shown in Fig. 5 in Methods together with the GEANT4 parametrization and the model employed in Ref. [28]. The same procedure is applied to describe the $^3\overline{\text{He}}$–^{4}He inelastic processes. These scaled inelastic cross sections have been implemented for the first time in GALPROP.

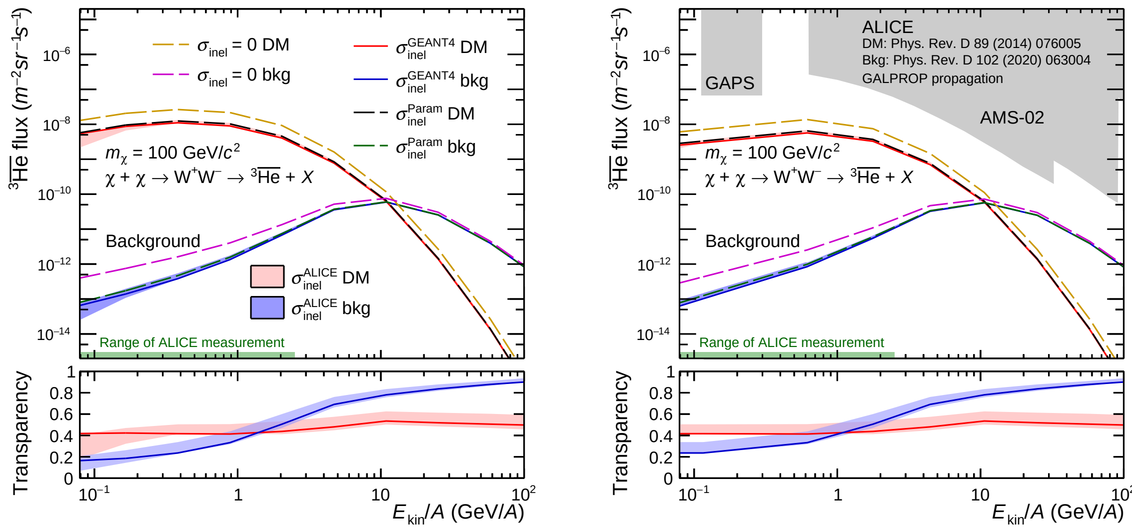

Fig. 4: Expected $^3\overline{\text{He}}$ flux near Earth before (left panel) and after (right panel) solar modulation. The latter is obtained using Force Field with modulation potential $\phi = 400$ MV. Upper panels show the fluxes for dark-matter signal χ (in red) and cosmic-ray background (in blue) antihelium nuclei for various cases of inelastic cross section used in the calculations. Bottom panels show the transparency of our galaxy to the propagation of $^3\overline{\text{He}}$ outside (left) and inside (right) the Solar System. Shaded areas on the top right panel show the expected sensitivity of the GAPS [73] and AMS-02 [28] experiments. The top panels also shows the fluxes obtained with $\sigma_{\text{inel}}(^3\overline{\text{He}})$ set to zero. Only the uncertainties relative to the measured $\sigma_{\text{inel}}(^3\overline{\text{He}})$ are shown.

The expected $^3\overline{\text{He}}$ flux near Earth after all propagation steps (Methods) with and without the effect of solar modulations is shown in the right and left panels of Fig. 4, respectively. The solar modulation is implemented using the Force Field method [67]. The effect of inelastic interactions is demonstrated showing the full propagation chain once with $\sigma_{\text{inel}}(^3\overline{\text{He}})$ set to zero and once with the inelastic cross section extracted from the ALICE measurement. Only the uncertainties relative to the measured $\sigma_{\text{inel}}(^3\overline{\text{He}})$ are propagated and presented in Fig. 4. It also shows the expected flux computed considering an alternative parametrization for $\sigma_{\text{inel}}(^3\overline{\text{He}})$ proposed in Ref. [28] (Methods). The resulting flux obtained with this parametrization is very similar to the results using $\sigma_{\text{inel}}(^3\overline{\text{He}})$ from GEANT4. The inelastic collisions of $^3\overline{\text{He}}$ with the interstellar gas lead to a significant reduction of the expected flux for both the signal candidates from dark matter and the background from cosmic-ray collisions.

The transparency of our galaxy to the $^3\overline{\mathrm{He}}$ passage is defined by the ratio of the flux obtained with and without inelastic processes in GALPROP. The transparency values as a function of the kinetic energy obtained with $\sigma_{\mathrm{inel}}(^3\overline{\mathrm{He}})$ from the GEANT4 parametrization and from the ALICE measurements are shown in the lower panels of Fig. 4 by the coloured lines and bands, respectively. The transparency profile at low kinetic energies ($\leq$ 300 MeV) outside the Solar System (bottom left panel of Fig. 4) is washed out by the solar modulation that shifts down the more abundant high-momentum particles to lower energies (bottom right panel in Fig. 4). A transparency of the galaxy of about 50% is estimated for $^3\overline{\mathrm{He}}$ from the considered dark-matter source [27] and of about 25% for low-energy $^3\overline{\mathrm{He}}$ from cosmic-ray interactions [51]. The latter increases further up to full transparency at higher energies. The different behaviour in the two cases is caused both by the different underlying spectral shape and by the different distribution of production points of the two sources, underlining the importance of full propagation studies. The employment of an alternative set of propagation parameters described in Ref. [74] results in $40-60\%$ lower transparency at low E_{kin} than using the propagation parameters from Ref. [40] (Methods).

The calculated $^3\overline{\mathrm{He}}$ transparency is found to be consistent, within its newly established uncertainties, with the GEANT4 parametrization. It must be clearly noted that previously it was not possible to quantify the uncertainty of the parametrizations employed in GEANT4 or proposed in Ref. [28] due to the lack of experimental data. In order to quantify the improvement originating from our study, we therefore simply compare the full difference between no inelastic interaction and the alternative parametrizations ($\sim$ 50% for the signal from dark matter and up to 75% for background) to our newly established uncertainties of about 10%–15% after the solar modulation. Note that the propagation example provided in this work does not cover the full range of uncertainties related to $^3\overline{\mathrm{He}}$ flux modelling (see the discussion in Methods), rather it delivers a clear road map for future studies. Since a large separation between signal and background is retained for low kinetic energies, our results clearly underline that the search for $^3\overline{\mathrm{He}}$ in space remains a very promising channel for the discovery of dark matter.

4 Summary

Studying antinuclei in laboratories on Earth and searching them in space belong to the most interesting research topics in modern nuclear and astroparticle physics. For the first observation of antinuclei in cosmic rays from dark matter, several ingredients have to be under precise control: their production mechanism, their interaction probability with the interstellar gas, and their detection in satellite or balloon experiments. Thanks to the unique capabilities of the ALICE experiment, we were able to quantify the inelastic cross section of $^3\overline{\mathrm{He}}$ based on experimental data. Our results confirm previous theoretical estimates and provide experimental uncertainties for $\sigma_{\mathrm{inel}}(^3\overline{\mathrm{He}})$ and the resulting transparency of our galaxy. A transparency of the galaxy of about 50% is estimated for the employed dark-matter source [27] and within 25%–90% for $^3\overline{\mathrm{He}}$ produced in cosmic-ray interactions [51] using the GALPROP code with propagation parameters from Ref. [40]. The associated uncertainties stemming only from the measurement presented in this paper are about 10%–15%. We have thus verified that the uncertainty related to nuclear absorption is subleading with respect to other possible contributions in the cosmic-ray and dark-matter modelling, in particular production mechanism and propagation description [27–29, 51]. The newly measured $\sigma_{\mathrm{inel}}(^3\overline{\mathrm{He}})$ and the developed methodology can be employed to carry out the propagation of $^3\overline{\mathrm{He}}$ using any dark-matter or cosmic-ray interaction modelling as a source. We found that $^3\overline{\mathrm{He}}$ nuclei can travel distances of several kpc in our galaxy without being absorbed and thus provide an excellent probe for new physics that awaits discovery.

Acknowledgements

The ALICE Collaboration would like to thank all its engineers and technicians for their invaluable contributions to the construction of the experiment and the CERN accelerator teams for the outstanding performance of the LHC complex. The ALICE Collaboration gratefully acknowledges the resources and support provided by all Grid centres and the Worldwide LHC Computing Grid (WLCG) collaboration. The ALICE Collaboration acknowledges the following funding agencies for their support in building and running the ALICE detector: A. I. Alikhanyan National Science Laboratory (Yerevan Physics Institute) Foundation (ANSL), State Committee of Science and World Federation of Scientists (WFS), Armenia; Austrian Academy of Sciences, Austrian Science Fund (FWF): [M 2467-N36] and Nationalstiftung für Forschung, Technologie und Entwicklung, Austria; Ministry of Communications and High Technologies, National Nuclear Research Center, Azerbaijan; Conselho Nacional de Desenvolvimento Científico e Tecnológico (CNPq), Financiadora de Estudos e Projetos (Finep), Fundação de Amparo à Pesquisa do Estado de São Paulo (FAPESP) and Universidade Federal do Rio Grande do Sul (UFRGS), Brazil; Ministry of Education of China (MOEC) , Ministry of Science & Technology of China (MSTC) and National Natural Science Foundation of China (NSFC), China; Ministry of Science and Education and Croatian Science Foundation, Croatia; Centro de Aplicaciones Tecnológicas y Desarrollo Nuclear (CEADEN), Cubaenergía, Cuba; Ministry of Education, Youth and Sports of the Czech Republic, Czech Republic; The Danish Council for Independent Research | Natural Sciences, the VILLUM FONDEN and Danish National Research Foundation (DNRF), Denmark; Helsinki Institute of Physics (HIP), Finland; Commissariat à l'Energie Atomique (CEA) and Institut National de Physique Nucléaire et de Physique des Particules (IN2P3) and Centre National de la Recherche Scientifique (CNRS), France; Bundesministerium für Bildung und Forschung (BMBF) and GSI Helmholtzzentrum für Schwerionenforschung GmbH, Germany; General Secretariat for Research and Technology, Ministry of Education, Research and Religions, Greece; National Research, Development and Innovation Office, Hungary; Department of Atomic Energy Government of India (DAE), Department of Science and Technology, Government of India (DST), University Grants Commission, Government of India (UGC) and Council of Scientific and Industrial Research (CSIR), India; Indonesian Institute of Science, Indonesia; Istituto Nazionale di Fisica Nucleare (INFN), Italy; Japanese Ministry of Education, Culture, Sports, Science and Technology (MEXT) and Japan Society for the Promotion of Science (JSPS) KAKENHI, Japan; Consejo Nacional de Ciencia (CONACYT) y Tecnología, through Fondo de Cooperación Internacional en Ciencia y Tecnología (FONCICYT) and Dirección General de Asuntos del Personal Academico (DGAPA), Mexico; Nederlandse Organisatie voor Wetenschappelijk Onderzoek (NWO), Netherlands; The Research Council of Norway, Norway; Commission on Science and Technology for Sustainable Development in the South (COMSATS), Pakistan; Pontificia Universidad Católica del Perú, Peru; Ministry of Education and Science, National Science Centre and WUT ID-UB, Poland; Korea Institute of Science and Technology Information and National Research Foundation of Korea (NRF), Republic of Korea; Ministry of Education and Scientific Research, Institute of Atomic Physics, Ministry of Research and Innovation and Institute of Atomic Physics and University Politehnica of Bucharest, Romania; Joint Institute for Nuclear Research (JINR), Ministry of Education and Science of the Russian Federation, National Research Centre Kurchatov Institute, Russian Science Foundation and Russian Foundation for Basic Research, Russia; Ministry of Education, Science, Research and Sport of the Slovak Republic, Slovakia; National Research Foundation of South Africa, South Africa; Swedish Research Council (VR) and Knut & Alice Wallenberg Foundation (KAW), Sweden; European Organization for Nuclear Research, Switzerland; Suranaree University of Technology (SUT), National Science and Technology Development Agency (NSDTA), Suranaree University of Technology (SUT), Thailand Science Research and Innovation (TSRI) and National Science, Research and Innovation Fund (NSRF), Thailand; Turkish Energy, Nuclear and Mineral Research Agency (TENMAK), Turkey; National Academy of Sciences of Ukraine, Ukraine; Science and Technology Facilities Council (STFC), United Kingdom; National Science Foundation of the United States of America (NSF) and United States Department of Energy, Office of Nuclear Physics (DOE NP),

United States of America.

References

[1] **NA44** Collaboration, J. Simon-Gillo *et al.*, "Deuteron and anti-deuteron production in CERN experiment NA44", *Nucl. Phys. A* **590** (1995) 483C–486C.

[2] **E864** Collaboration, T. Armstrong *et al.*, "Anti-deuteron yield at the AGS and coalescence implications", *Phys. Rev. Lett.* **85** (2000) 2685–2688, `arXiv:nucl-ex/0005001`.

[3] **NA49** Collaboration, S. Afanasiev *et al.*, "Deuteron production in central Pb + Pb collisions at 158-A-GeV", *Phys. Lett. B* **486** (2000) 22–28.

[4] **NA49** Collaboration, T. Anticic *et al.*, "Energy and centrality dependence of deuteron and proton production in Pb + Pb collisions at relativistic energies", *Phys. Rev. C* **69** (2004) 024902.

[5] **PHENIX** Collaboration, S. Adler *et al.*, "Deuteron and antideuteron production in Au + Au collisions at $\sqrt{s_{\mathrm{NN}}}$ = 200 GeV", *Phys. Rev. Lett.* **94** (2005) 122302, `arXiv:nucl-ex/0406004`.

[6] B. Alper *et al.*, "Large angle production of stable particles heavier than the proton and a search for quarks at the cern intersecting storage rings", *Phys. Lett. B* **46** (1973) 265–268.

[7] **British-Scandinavian-MIT** Collaboration, S. Henning *et al.*, "Production of Deuterons and anti-Deuterons in Proton Proton Collisions at the CERN ISR", *Lett. Nuovo Cim.* **21** (1978) 189.

[8] T. Alexopoulos *et al.*, "Cross-sections for deuterium, tritium, and helium production in $\bar{p}p$ collisions at $\sqrt{s}$ = 1.8 TeV", *Phys. Rev. D* **62** (2000) 072004.

[9] **H1** Collaboration, A. Aktas *et al.*, "Measurement of anti-deuteron photoproduction and a search for heavy stable charged particles at HERA", *Eur. Phys. J. C* **36** (2004) 413–423, `arXiv:hep-ex/0403056`.

[10] **CLEO** Collaboration, D. Asner *et al.*, "Anti-deuteron production in $\Upsilon(nS)$ decays and the nearby continuum", *Phys. Rev. D* **75** (2007) 012009, `arXiv:hep-ex/0612019`.

[11] **ALEPH** Collaboration, S. Schael *et al.*, "Deuteron and anti-deuteron production in $e^{+}e^{-}$ collisions at the Z resonance", *Phys. Lett. B* **639** (2006) 192–201, `arXiv:hep-ex/0604023`.

[12] **ALICE** Collaboration, J. Adam *et al.*, "Production of light nuclei and anti-nuclei in pp and Pb–Pb collisions at energies available at the CERN Large Hadron Collider", *Phys. Rev.* **C93** (2016) 024917, `arXiv:1506.08951 [nucl-ex]`.

[13] **ALICE** Collaboration, J. Adam *et al.*, "$^{3}_{\Lambda}\mathrm{H}$ and $^{3}_{\bar{\Lambda}}\overline{\mathrm{H}}$ production in Pb–Pb collisions at $\sqrt{s_{\mathrm{NN}}} = 2.76$ TeV", *Phys. Lett.* **B754** (2016) 360–372, `arXiv:1506.08453 [nucl-ex]`.

[14] **ALICE** Collaboration, S. Acharya *et al.*, "Measurement of deuteron spectra and elliptic flow in Pb–Pb collisions at $\sqrt{s_{\mathrm{NN}}}$ = 2.76 TeV at the LHC", *Eur. Phys. J.* **C77** (2017) 658, `arXiv:1707.07304 [nucl-ex]`.

[15] **ALICE** Collaboration, S. Acharya *et al.*, "Multiplicity dependence of (anti-)deuteron production in pp collisions at $\sqrt{s}$ = 7 TeV", *Phys. Lett.* **B794** (2019) 50–63, `arXiv:1902.09290 [nucl-ex]`.

[16] **STAR** Collaboration, H. Agakishiev *et al.*, "Observation of the antimatter helium-4 nucleus", *Nature* **473** (2011) 353, `arXiv:1103.3312 [nucl-ex]`.

[17] **STAR** Collaboration, B. I. Abelev *et al.*, "Observation of an Antimatter Hypernucleus", *Science* **328** (2010) 58–62, arXiv:1003.2030 [nucl-ex].

[18] **ALICE** Collaboration, J. Adam *et al.*, "Precision measurement of the mass difference between light nuclei and anti-nuclei", *Nature Phys.* **11** (2015) 811–814, arXiv:1508.03986 [nucl-ex].

[19] **STAR** Collaboration, J. Adam *et al.*, "Measurement of the mass difference and the binding energy of the hypertriton and antihypertriton", *Nature Phys.* **16** (2020) 409–412, arXiv:1904.10520 [hep-ex].

[20] A. Ibarra and S. Wild, "Prospects of antideuteron detection from dark matter annihilations or decays at AMS-02 and GAPS", *JCAP* **02** (2013) 021, arXiv:1209.5539 [hep-ph].

[21] M. Persic, P. Salucci, and F. Stel, "The Universal rotation curve of spiral galaxies: 1. The Dark matter connection", *Mon. Not. Roy. Astron. Soc.* **281** (1996) 27, arXiv:astro-ph/9506004.

[22] V. Poulin, P. Salati, I. Cholis, M. Kamionkowski, and J. Silk, "Where do the AMS-02 antihelium events come from?", *Phys. Rev. D* **99** (2019) 023016, arXiv:1808.08961 [astro-ph.HE].

[23] **Planck** Collaboration, N. Aghanim *et al.*, "Planck 2018 results. VI. Cosmological parameters", *Astron. Astrophys.* **641** (2020) A6, arXiv:1807.06209 [astro-ph.CO].

[24] D. Clowe, M. Bradac, A. H. Gonzalez, M. Markevitch, S. W. Randall, C. Jones, and D. Zaritsky, "A direct empirical proof of the existence of dark matter", *Astrophys. J. Lett.* **648** (2006) L109–L113, arXiv:astro-ph/0608407.

[25] J. Bond and G. Efstathiou, "Cosmic background radiation anisotropies in universes dominated by nonbaryonic dark matter", *Astrophys. J. Lett.* **285** (1984) L45–L48.

[26] **Boomerang** Collaboration, P. de Bernardis *et al.*, "A Flat universe from high resolution maps of the cosmic microwave background radiation", *Nature* **404** (2000) 955–959, arXiv:astro-ph/0004404.

[27] E. Carlson, A. Coogan, T. Linden, S. Profumo, A. Ibarra, and S. Wild, "Antihelium from Dark Matter", *Phys. Rev. D* **89** (2014) 076005, arXiv:1401.2461 [hep-ph].

[28] M. Korsmeier, F. Donato, and N. Fornengo, "Prospects to verify a possible dark matter hint in cosmic antiprotons with antideuterons and antihelium", *Phys. Rev.* **D97** (2018) 103011, arXiv:1711.08465 [astro-ph.HE].

[29] P. von Doetinchem *et al.*, "Cosmic-ray antinuclei as messengers of new physics: status and outlook for the new decade", *JCAP* **08** (2020) 035, arXiv:2002.04163 [astro-ph.HE].

[30] M. W. Winkler and T. Linden, "Dark Matter Annihilation Can Produce a Detectable Antihelium Flux through $\bar{\Lambda}_b$ Decays", *Phys. Rev. Lett.* **126** no. 10, (2021) 101101, arXiv:2006.16251 [hep-ph].

[31] F. Bellini, K. Blum, A. P. Kalweit, and M. Puccio, "Examination of coalescence as the origin of nuclei in hadronic collisions", *Phys. Rev. C* **103** (2021) 014907, arXiv:2007.01750 [nucl-th].

[32] M. Kachelriess, S. Ostapchenko, and J. Tjemsland, "On nuclear coalescence in small interacting systems", *Eur. Phys. J. A* **57** (2021) 167, arXiv:2012.04352 [hep-ph].

[33] P. Braun-Munzinger and B. Dönigus, "Loosely-bound objects produced in nuclear collisions at the LHC", *Nucl. Phys. A* **987** (2019) 144–201, arXiv:1809.04681 [nucl-ex].

[34] J. Steinheimer, K. Gudima, A. Botvina, I. Mishustin, M. Bleicher, and H. Stocker, "Hypernuclei, dibaryon and antinuclei production in high energy heavy ion collisions: Thermal production versus Coalescence", *Phys. Lett. B* **714** (2012) 85–91, `arXiv:1203.2547 [nucl-th]`.

[35] P. Braun-Munzinger and J. Stachel, "Production of strange clusters and strange matter in nucleus-nucleus collisions at the AGS", *J. Phys. G* **21** (1995) L17–L20, `arXiv:nucl-th/9412035`.

[36] A. Andronic, P. Braun-Munzinger, J. Stachel, and H. Stoecker, "Production of light nuclei, hypernuclei and their antiparticles in relativistic nuclear collisions", *Phys. Lett.* **B697** (2011) 203–207, `arXiv:1010.2995 [nucl-th]`.

[37] J. Cleymans, S. Kabana, I. Kraus, H. Oeschler, K. Redlich, *et al.*, "Antimatter production in proton-proton and heavy-ion collisions at ultrarelativistic energies", *Phys. Rev.* **C84** (2011) 054916, `arXiv:1105.3719 [hep-ph]`.

[38] S. Butler and C. Pearson, "Deuterons from High-Energy Proton Bombardment of Matter", *Phys. Rev.* **129** (1963) 836–842.

[39] R. Scheibl and U. W. Heinz, "Coalescence and flow in ultrarelativistic heavy ion collisions", *Phys. Rev.* **C59** (1999) 1585–1602, `arXiv:nucl-th/9809092 [nucl-th]`.

[40] M. Boschini *et al.*, "Inference of the Local Interstellar Spectra of Cosmic-Ray Nuclei Z $\leq$ 28 with the GalProp–HelMod Framework", *Astrophys. J. Suppl.* **250** (2020) 27, `arXiv:2006.01337 [astro-ph.HE]`.

[41] **ALICE** Collaboration, E. Abbas *et al.*, "Mid-rapidity anti-baryon to baryon ratios in pp collisions at $\sqrt{s}$ = 0.9, 2.76 and 7 TeV measured by ALICE", *Eur. Phys. J. C* **73** (2013) 2496, `arXiv:1305.1562 [nucl-ex]`.

[42] **ALICE** Collaboration, S. Acharya *et al.*, "Measurement of the low-energy antideuteron inelastic cross section", *Phys. Rev. Lett.* **125** (2020) 162001, `arXiv:2005.11122 [nucl-ex]`.

[43] **ALICE** Collaboration, K. Aamodt *et al.*, "The ALICE experiment at the CERN LHC", *JINST* **3** (2008) S08002.

[44] **ALICE** Collaboration, B. Abelev *et al.*, "Performance of the ALICE Experiment at the CERN LHC", *Int. J. Mod. Phys.* **A29** (2014) 1430044, `arXiv:1402.4476 [nucl-ex]`.

[45] **ALICE** Collaboration, K. Aamodt *et al.*, "Midrapidity antiproton-to-proton ratio in pp collisions at $\sqrt{s} = 0.9$ and 7 TeV measured by the ALICE experiment", *Phys. Rev. Lett.* **105** (2010) 072002, `arXiv:1006.5432 [hep-ex]`.

[46] See Supplemental Material for cumulative distribution of the material in the ALICE apparatus at http://link.aps.org/supplemental/10.1103/PhysRevLett.125.162001.

[47] **GEANT4** Collaboration, S. Agostinelli *et al.*, "GEANT4: A Simulation toolkit", *Nucl.Instrum.Meth.* **A506** (2003) 250–303.

[48] V. Uzhinsky, J. Apostolakis, A. Galoyan, G. Folger, V. Grichine, *et al.*, "Antinucleus-nucleus cross sections implemented in GEANT4", *Phys. Lett.* **B705** (2011) 235–239.

[49] J. H. Lambert, *Photometria, sive De mensura et gradibus luminis, colorum et umbrae.* 1760.

[50] J. Cudell, V. Ezhela, P. Gauron, K. Kang, Y. Kuyanov, S. Lugovsky, B. Nicolescu, and N. Tkachenko, "Hadronic scattering amplitudes: Medium-energy constraints on asymptotic behavior", *Phys. Rev. D* **65** (2002) 074024, `arXiv:hep-ph/0107219`.

[51] A. Shukla, A. Datta, P. von Doetinchem, D.-M. Gomez-Coral, and C. Kanitz, "Large-scale Simulations of Antihelium Production in Cosmic-ray Interactions", *Phys. Rev. D* **102** (2020) 063004, arXiv:2006.12707 [astro-ph.HE].

[52] **ALICE** Collaboration, J. Adam *et al.*, "Production of light nuclei and anti-nuclei in pp and Pb–Pb collisions at energies available at the CERN Large Hadron Collider", *Phys. Rev. C* **93** (2016) 024917, arXiv:1506.08951 [nucl-ex].

[53] N. Tomassetti and A. Oliva, "Production and acceleration of antinuclei in supernova shockwaves", *Astrophys. J. Lett.* **844** no. 2, (2017) L26, arXiv:1707.06915 [astro-ph.HE].

[54] J. Herms, A. Ibarra, A. Vittino, and S. Wild, "Antideuterons in cosmic rays: sources and discovery potential", *JCAP* **02** (2017) 018, arXiv:1610.00699 [astro-ph.HE].

[55] A. Barrau, G. Boudoul, F. Donato, D. Maurin, P. Salati, I. Stefanon, and R. Taillet, "Antideuterons as a probe of primordial black holes", *Astron. Astrophys.* **398** (2003) 403–410, arXiv:astro-ph/0207395.

[56] L. Šerkšnytė *et al.*, "Reevaluation of the cosmic antideuteron flux from cosmic-ray interactions and from exotic sources", arXiv:2201.00925 [astro-ph.HE].

[57] J. F. Navarro, C. S. Frenk, and S. D. White, "The Structure of cold dark matter halos", *Astrophys. J.* **462** (1996) 563–575, arXiv:astro-ph/9508025.

[58] R. Kissmann, "Galactic cosmic ray propagation models using picard", *Journal of Physics: Conference Series* **837** (May, 2017) 012003. https://doi.org/10.1088/1742-6596/837/1/012003.

[59] R. Kissmann, "PICARD: A novel code for the Galactic Cosmic Ray propagation problem", *Astropart. Phys.* **55** (2014) 37–50, arXiv:1401.4035 [astro-ph.HE].

[60] C. Evoli, D. Gaggero, D. Grasso, and L. Maccione, "Cosmic ray nuclei, antiprotons and gamma rays in the galaxy: a new diffusion model", *Journal of Cosmology and Astroparticle Physics* **2008** (Oct, 2008) 018. https://doi.org/10.1088/1475-7516/2008/10/018.

[61] A. Strong and I. Moskalenko, "Propagation of cosmic-ray nucleons in the galaxy", *Astrophys. J.* **509** (1998) 212–228, arXiv:astro-ph/9807150.

[62] I. V. Moskalenko, A. W. Strong, J. F. Ormes, and M. S. Potgieter, "Secondary anti-protons and propagation of cosmic rays in the galaxy and heliosphere", *Astrophys. J.* **565** (2002) 280–296, arXiv:astro-ph/0106567.

[63] L. Bronfman, R. S. Cohen, H. Alvarez, J. May, and P. Thaddeus, "A CO Survey of the Southern Milky Way: The Mean Radial Distribution of Molecular Clouds within the Solar Circle", *Astrophysical Journal* **324** (Jan., 1988) 248.

[64] M. A. Gordon and W. B. Burton, "Carbon monoxide in the Galaxy. I. The radial distribution of CO, H_2, and nucleons.", *Astrophysical Journal* **208** (Sept., 1976) 346–353.

[65] J. M. Cordes, J. M. Weisberg, D. A. Frail, S. R. Spangler, and M. Ryan, "The galactic distribution of free electrons", *Nature* **354** (Nov., 1991) 121–124.

[66] J. M. Dickey and F. J. Lockman, "H I in the galaxy.", *Annual Review of Astronomy and Astrophysics* **28** (Jan., 1990) 215–261.

[67] L. Gleeson and W. Axford, “Solar Modulation of Galactic Cosmic Rays”, *Astrophys. J.* **154** (1968) 1011.

[68] M. J. Boschini, S. Della Torre, M. Gervasi, G. La Vacca, and P. G. Rancoita, “The HelMod Model in the Works for Inner and Outer Heliosphere: from AMS to Voyager Probes Observations”, *Adv. Space Res.* **64** (2019) 2459–2476, arXiv:1903.07501 [physics.space-ph].

[69] A. Cummings, E. Stone, B. Heikkila, N. Lal, W. Webber, G. Jóhannesson, I. Moskalenko, E. Orlando, and T. Porter, “Galactic Cosmic Rays in the Local Interstellar Medium: Voyager 1 Observations and Model Results”, *Astrophys. J.* **831** (2016) 18.

[70] **AMS** Collaboration, M. Aguilar *et al.*, “Precision Measurement of the Proton Flux in Primary Cosmic Rays from Rigidity 1 GV to 1.8 TV with the Alpha Magnetic Spectrometer on the International Space Station”, *Phys. Rev. Lett.* **114** (2015) 171103.

[71] J. Engelmann, P. Ferrando, A. Soutoul, P. Goret, and E. Juliusson, “Charge composition and energy spectra of cosmic-ray for elements from Be to NI - Results from HEAO-3-C2”, *Astron. Astrophys.* **233** (1990) 96–111.

[72] H. Ahn *et al.*, “Measurements of cosmic-ray secondary nuclei at high energies with the first flight of the CREAM balloon-borne experiment”, *Astropart. Phys.* **30** (2008) 133–141, arXiv:0808.1718 [astro-ph].

[73] **GAPS** Collaboration, N. Saffold *et al.*, “Cosmic antihelium-3 nuclei sensitivity of the GAPS experiment”, *Astropart. Phys.* **130** (2021) 102580, arXiv:2012.05834 [hep-ph].

[74] A. Cuoco, M. Krämer, and M. Korsmeier, “Novel Dark Matter Constraints from Antiprotons in Light of AMS-02”, *Phys. Rev. Lett.* **118** no. 19, (2017) 191102, arXiv:1610.03071 [astro-ph.HE].

[75] **ALICE** Collaboration, J. Adam *et al.*, “Pseudorapidity and transverse-momentum distributions of charged particles in proton–proton collisions at $\sqrt{s} = 13$ TeV”, *Phys. Lett. B* **753** (2016) 319–329, arXiv:1509.08734 [nucl-ex].

[76] **ALICE** Collaboration, J. Adam *et al.*, “Centrality dependence of the charged-particle multiplicity density at midrapidity in Pb-Pb collisions at $\sqrt{s_{\mathrm{NN}}}$ = 5.02 TeV”, *Phys. Rev. Lett.* **116** (2016) 222302, arXiv:1512.06104 [nucl-ex].

[77] **ALICE** Collaboration, “Validation of the ALICE material budget between TPC and TOF detectors”, *ALICE-PUBLIC-2022-001* (Feb, 2022) . https://cds.cern.ch/record/2800896.

[78] **Particle Data Group** Collaboration, P. A. Zyla *et al.*, “Review of Particle Physics”, *PTEP* **2020** (2020) 083C01.

[79] A. Ingemarsson *et al.*, “Reaction cross sections of intermediate energy 3 He-particles on targets from 9 Be to 208 Pb”, *Nucl. Phys. A* **696** (2001) 3–30.

[80] H.-N. Lin and X. Li, “The Dark Matter Profiles in the Milky Way”, *Mon. Not. Roy. Astron. Soc.* **487** (2019) 5679–5684, arXiv:1906.08419 [astro-ph.GA].

[81] **ALICE** Collaboration, “Modelling of Antihelium-3 Cosmic-Ray Propagation”, *ALICE-PUBLIC-2022-002* (Feb, 2022) . https://cds.cern.ch/record/2800897.

[82] D.-M. Gomez-Coral, A. Menchaca Rocha, V. Grabski, A. Datta, P. von Doetinchem, and A. Shukla, “Deuteron and Antideuteron Production Simulation in Cosmic-Ray Interactions”, *Phys. Rev. D* **98** (2018) 023012, arXiv:1806.09303 [astro-ph.HE].

[83] **ALICE** Collaboration, S. Acharya *et al.*, “Production of deuterons, tritons, ^{3}He nuclei and their antinuclei in pp collisions at $\sqrt{s}$ = 0.9, 2.76 and 7 TeV”, *Phys. Rev.* **C97** (2018) 024615, arXiv:1709.08522 [nucl-ex].

[84] **ALICE** Collaboration, S. Acharya *et al.*, “(Anti-)deuteron production in pp collisions at $\sqrt{s} = 13$ TeV”, *Eur. Phys. J. C* **80** (2020) 889, arXiv:2003.03184 [nucl-ex].

[85] T. Sjostrand, S. Mrenna, and P. Z. Skands, “A Brief Introduction to PYTHIA 8.1”, *Comput. Phys. Commun.* **178** (2008) 852–867, arXiv:0710.3820 [hep-ph].

[86] A. Burkert, “The Structure of dark matter halos in dwarf galaxies”, *Astrophys. J. Lett.* **447** (1995) L25, arXiv:astro-ph/9504041.

[87] K. G. Begeman, A. H. Broeils, and R. H. Sanders, “Extended rotation curves of spiral galaxies: Dark haloes and modified dynamics”, *Mon. Not. Roy. Astron. Soc.* **249** (1991) 523.

5 Methods

5.1 Event selection

The inelastic pp and Pb–Pb events were recorded with the ALICE apparatus at collision energies of $\sqrt{s} = 13$ TeV and $\sqrt{s_{\mathrm{NN}}} = 5.02$ TeV, respectively. Events are triggered by the V0 detector comprising two plastic scintillator arrays placed on both sides of the interaction point and covering the pseudorapidity intervals of $2.8 < \eta < 5.1$ and $-3.7 < \eta < -1.7$. The pseudorapidity is defined as $\eta = -\ln[\tan(\frac{\Theta}{2})]$ with Θ being the polar angle of the particle with respect to the beam axis. The trigger condition is defined by the coincidence of signals in both arrays of the V0 detector. Together with two innermost layers of the ITS detector, the V0 is also used to reject background events like beam–gas interactions or collisions with mechanical structures of the beam line. For the analysis of pp data, a high-multiplicity trigger is employed to select only events with the total signal amplitude measured in the V0 detector above a certain threshold, which leads to a selection of about 0.17% of the inelastic pp collisions with the highest V0 signal. In these events the number of charged particles produced at midrapidity $|\eta| < 0.5$ is about 6 times higher than $\langle \mathrm{d}N_{\mathrm{ch}}/\mathrm{d}y \rangle = 5.31 \pm 0.18$ measured in inelastic pp collision at $\sqrt{s} = 13$ TeV [75]. This facilitates the analysis of rarely produced (anti)^{3}He nuclei. As for Pb–Pb experimental data, 10% of all inelastic events with the highest signal amplitude in the V0 detector are considered for the analysis. In these events the average charged-particle multiplicity at midrapidity $|\eta| < 0.5$ amounts to $\langle \mathrm{d}N_{\mathrm{ch}}/\mathrm{d}y \rangle = 1764 \pm 50$ [76]. In total 147.9×10^6 Pb–Pb and 10^9 pp events were analysed.

5.2 Particle tracking and identification

Trajectories of charged particles are reconstructed in the ALICE central barrel from their hits in the Inner Tracking System (ITS) and Time Projection Chamber (TPC). The detectors are located inside a solenoidal magnetic field (0.5 T) bending the trajectories of charged particles. The curvature and direction of the charged-particle trajectories in the magnetic field is used to reconstruct their momentum. The detectors provide full azimuthal coverage in the pseudorapidity interval $|\eta| < 0.9$. This η range corresponds to the region within ± 42 degrees of the transverse plane that is perpendicular to the beam axis. Typical resolution of the transverse momentum reconstructed at the primary vertex ($p_{\mathrm{T,primary}}$) for protons, pions and kaons varies from about 2% for tracks with $p_{\mathrm{T,primary}} = 10$ GeV/c to below 1% for $p_{\mathrm{T,primary}} \leq 1$ GeV/c.

Specific energy loss in the TPC gas is used to identify charged particles. Due to their electric charge $= 2$, high mass and the quadratic dependence of the specific energy loss on the particle charge, ^{3}He and $^3\overline{\mathrm{He}}$ nuclei have larger energy loss than most of other (anti)particles produced in the collision (like pions, kaons, protons and deuterons) and can be clearly identified in the TPC. The selected ^{3}He candidates include substantial amount of background from secondary nuclei which originate from spallation reactions in the detector material. This contribution is estimated via a fit to the distribution of the measured distance of closest approach (DCA) between track candidates and the primary collision vertex using templates from Monte Carlo simulations. Since primary particles point back to the primary vertex, they are characterized by a distinct peak structure at zero DCA, whereas secondary particles correspond to a flat DCA distribution and their contribution can therefore be separated. More details on this procedure can be found in Ref. [41, 52]. For ^{3}He candidates in pp collisions at $\sqrt{s} = 13$ TeV this contribution amounts to $\sim 75\%$ in the lowest analysed momentum interval $0.65 \leq p_{\mathrm{primary}}/z < 0.8$ GeV/c and is negligible in the momentum range above $p_{\mathrm{primary}}/z = 1.5$ GeV/c. For $^3\overline{\mathrm{He}}$ nuclei there is no contribution from spallation processes. In total there are 16801 ± 130 primary $^3\overline{\mathrm{He}}$ reconstructed in the TPC in the Pb–Pb data sample. In the sample of pp collisions, the total number of reconstructed primary candidates amounts to 773 ± 46 ^{3}He and 652 ± 30 $^3\overline{\mathrm{He}}$. The uncertainties for these values result from the fit to the TPC signal which is used to reject (small) background from (anti)triton nuclei misidentified as (anti)^{3}He at low momenta.

5.3 Corrections and evaluation of the systematic uncertainties

Due to continuous energy-loss effects in the detector material, inelastic interaction of $^3\overline{\mathrm{He}}$ with the detector material happens at a momentum p, which is lower than the momentum p_{primary} reconstructed at the primary collision vertex. The corresponding effect is taken into account utilising Monte Carlo (MC) simulations in which one has precise information about both momenta for each (anti)particle. In the analysis of pp collisions, the average values of p/p_{primary} distributions in each analysed p_{primary} interval are used to consider the energy loss. The root mean square (RMS) of these distributions is used to determine the uncertainty of the momentum p, which is propagated to the uncertainty of the measured cross section. For the analysis of Pb–Pb data sample, the MC information on the momenta of daughter tracks originating from the $^3\overline{\mathrm{He}}$ annihilation is used to estimate the corresponding effect and the resulting uncertainty.

The systematic uncertainties due to tracking, particle identification and the description of material budget in MC simulations are considered, and the total uncertainty is obtained as the quadratic sum of the individual contributions. The material budget of the ALICE apparatus [46] is varied by $\pm 4.5\%$ in MC simulations, and the deviations of the final results from the default case are considered as an uncertainty. The precision of $\sim 4.5\%$ of the MC parametrization is validated for the ALICE material with photon conversion analyses (up to the outer TPC vessel [44]) and with tagged pion and proton absorption studies (for the material between TPC and TOF detectors [77]).

For the Pb–Pb analysis the total systematic uncertainty amounts to $\sim 20\%$ in the highest and lowest momentum intervals considered in the analysis and decreases to $\leq 10\%$ in the momentum interval of $3 \leq p < 7$ GeV/c. For the analysis of pp data which is based on the antibaryon-to-baryon ratio method, an additional uncertainty due to primordial antibaryon-to-baryon ratio produced in collisions is considered as a global uncertainty. The primordial antiproton-to-proton ratio of 0.998 ± 0.015 is extrapolated for $\sqrt{s} = 13$ TeV collision energy from available measurements [41, 45], and, under the assumption that the (anti)^{3}He yield is proportional to the cube of (anti)proton yield [39], the primary $^3\overline{\mathrm{He}}/^3\mathrm{He}$ ratio amounts to 0.994 ± 0.045. This uncertainty is the dominant contribution to the total systematic uncertainty for the pp analysis which amounts to $\sim 8\%$.

5.4 Monte Carlo Simulation

The results presented in this paper are compared with detailed MC simulations of the ALICE detector. The simulations start with the generation of (anti)particles at the primary collision vertex and the production of raw detector information, taking into account also inactive subdetector channels. The same reconstruction algorithms applied to real experimental data are employed to analyse the raw simulated data. For the pp analysis based on antimatter-to-matter ratio, the primordial $^3\overline{\text{He}}/^3\text{He}$ ratio of 0.994 is used as an input for the MC simulations. For the propagation of (anti)particles through the detector material the simulations rely on the GEANT4 software package [47], in which the inelastic cross section of $^3\overline{\text{He}}$ nuclei is based on Glauber calculations. Since the Glauber model simulations are computationally too extensive to be performed during the propagation steps through the material, they are parameterized as a function of the atomic mass number A of the target nucleus as described in Ref. [48]:

$$\sigma_{hA}^{\text{inel}} = \pi R_A^2 \ln\left(1 + \frac{A\sigma_{hN}^{\text{tot}}}{\pi R_A^2}\right). \tag{1}$$

Here h denotes the nucleus in question (the formula is used for h = $\overline{\text{p}}$, $\overline{\text{d}}$, $^3\overline{\text{He}}$ and $^4\overline{\text{He}}$), and A is the atomic number of the target nucleus with radius R_A. σ_{hN}^{tot} is the total (elastic plus inelastic) cross section of hadron h on nucleon N, which is estimated with the help of Glauber calculations by extrapolating the measured $\overline{\text{p}}\text{p}$ values [50] to larger antinuclei. We performed several full-scale Monte Carlo simulations with varied inelastic cross sections of $^3\overline{\text{He}}$ with matter, and the simulated observables used in this analysis are studied as a function of the inelastic cross section re-scaling. This dependence is parametrized using the Lambert–Beer law as shown in panels (e) and (f) in Fig. 1. The parametrization reads as $N_{\text{surv}} = N_0 \times \exp(-\sigma_{\text{inel}}\rho L)$, where N_0 corresponds to the number of incident particles, N_{surv} to the number of survived particles that did not get absorbed, σ_{inel} to the inelastic cross section, ρ to the density of the material crossed, and L to the length of the particle trajectory in the material. The free parameter given by the product of ρL is determined by a fit to the simulated observables.

In order to model the inelastic cross section of $^3\overline{\text{He}}$ nuclei in the interstellar medium, the GEANT4 parametrization of the $^3\overline{\text{He}}$–p inelastic cross section are scaled with the correction factors obtained from the ALICE measurements. The additional uncertainty that originates from re-scaling a measurement at $\langle A\rangle = 17.4$ and $\langle A\rangle = 34.7$ to $A = 1$ and $A = 4$ is taken from the difference between the parametrization for the dependence on A in GEANT4 and in full Glauber calculation and amounts to $< 8\%$ [48]. The resulting $^3\overline{\text{He}}$–p inelastic cross section is shown in Fig. 5 together with the model employed in Ref. [28]. The latter is based on the approximation which uses available measurements to estimate the inelastic antideuteron–proton cross section in the following way:

$$\sigma_{\text{inel}}^{\overline{\text{d}}\text{p}} \approx \frac{\sigma_{\text{tot}}^{\overline{\text{d}}\text{p}}}{\sigma_{\text{tot}}^{\overline{\text{p}}\text{p}}}(\sigma_{\text{tot}}^{\overline{\text{p}}\text{p}} - \sigma_{\text{el}}^{\overline{\text{p}}\text{p}}). \tag{2}$$

By symmetry the total antideuteron–proton cross section $\sigma_{\text{tot}}^{\overline{\text{d}}\text{p}}$ is equal to the total deuteron–antiproton cross section which is taken from Ref. [78]. For antihelium the inelastic cross section is scaled from antideuterons according to the mass number as $\sigma_{\text{inel}}^{^3\overline{\text{He}}\text{p}} = \frac{3}{2}\sigma_{\text{inel}}^{\overline{\text{d}}\text{p}}$.

The results on inelastic $^3\overline{\text{He}}$ cross section are also tested against the modifications of elastic cross sections of $^3\overline{\text{He}}$ nuclei. Both ^{3}He and $^3\overline{\text{He}}$ elastic cross sections are varied independently by 30%, which led to $\leq 1\%$ modifications of the final results. For the analysis of proton–proton collisions based on the antibaryon-to-baryon ratio method, the results are additionally investigated for the sensitivity to the ^{3}He inelastic cross section. The latter is varied by 10% which is the uncertainty of the GEANT4 parametrizations obtained from fits to experimental data [79]. This variation yields a modification of $\leq 2.3\%$ in the reconstructed antihelium-to-helium ratio.

5.5 Propagation modelling

The possible sources of antinuclei in our galaxy are either cosmic-ray interactions with nuclei in the interstellar gas or more exotic sources such as dark-matter annihilations or decays. Cosmic rays consist

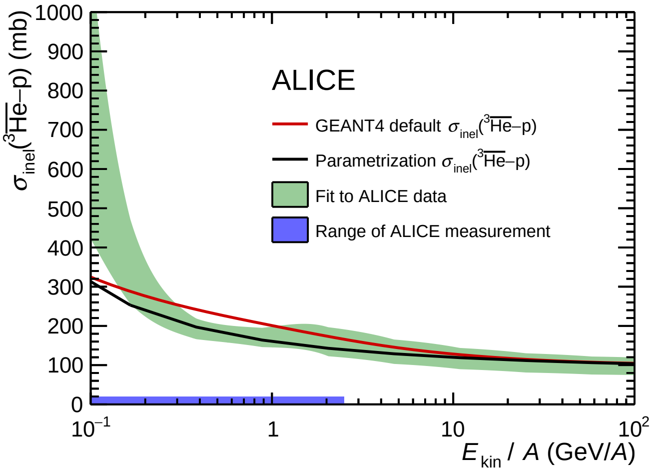

Fig. 5: Inelastic cross section for $^{3}\overline{\mathrm{He}}$ on protons. The green band shows the scaled ALICE measurement (see text for details), the red line represents the original GEANT4 parametrization and the black line the parametrization employed in Ref. [28]. The blue band on the x axis indicates the kinetic energy range corresponding to the ALICE measurement for $\sigma_{\mathrm{inel}}(^{3}\overline{\mathrm{He}})$.

mainly of protons and originate from supernovae remnants while dark matter so far escaped direct or indirect detection but its density profile can be modelled [80].

The propagation in the galaxy can be carried out using the publicly available propagation models [58–61]. We choose the GALPROP code (version 56) for the implementation of $^{3}\overline{\mathrm{He}}$ cosmic-ray propagation, which is discussed in details in [81]. GALPROP numerically solves a general transport equation for all included particle species [61]. This transport equation reads as

$$\frac{\partial\psi}{\partial t} = q(\mathbf{r},p) + \nabla\cdot(D_{xx}\mathbf{grad}\,\psi - \mathbf{V}\psi) + \frac{\partial}{\partial p}p^2 D_{pp}\frac{\partial}{\partial p}\frac{\psi}{p^2} - \frac{\partial}{\partial p}\left[\psi\frac{\mathrm{d}p}{\mathrm{d}t} - \frac{p}{3}(\nabla\cdot\mathbf{V})\psi\right] - \frac{\psi}{\tau}. \quad (3)$$

Here, $\psi = \psi(\mathbf{r},p,t)$ is the time dependent $^{3}\overline{\mathrm{He}}$ density per unit of the total particle momentum and $q(\mathbf{r},p)$ is the source function for $^{3}\overline{\mathrm{He}}$. The second and third terms describe the propagation of $^{3}\overline{\mathrm{He}}$ where the D_{xx}, $\mathbf{V}$ and D_{pp} are the spatial diffusion coefficient, convection velocity and the diffusive re-acceleration coefficient, respectively. While the effect of the galactic magnetic field is not explicitly modelled, it is accounted for by these terms of the transport equation. These coefficients are the same for all particle species and can be constrained using available cosmic-ray measurements. We use the best fit values of these parameters provided in Ref. [40]. The fourth term accounts for momentum losses via cosmic-ray interactions with interstellar gas ($\mathrm{d}p/\mathrm{d}t$) and the adiabatic momentum losses ($\nabla\cdot\mathbf{V}$). The last term represents the $^{3}\overline{\mathrm{He}}$ inelastic collisions with interstellar gas, where $1/\tau$ is the fragmentation rate. It is related to the inelastic cross section as:

$$\frac{1}{\tau} = \beta c\left(n_H(\mathbf{r})\sigma_{\mathrm{inel}}^{^{3}\overline{\mathrm{He}}\mathrm{p}}(p) + n_{He}(\mathbf{r})\sigma_{\mathrm{inel}}^{^{3}\overline{\mathrm{He}}^{4}\mathrm{He}}(p)\right) \quad (4)$$

Only the first and last terms require particle specific information. $^{3}\overline{\mathrm{He}}$ nuclei can be produced when cosmic-ray (CR) particles interact with protons or ^{4}He nuclei in the interstellar medium (ISM). The $^{3}\overline{\mathrm{He}}$ source function in this case is:

$$q(\mathbf{r},p) = \sum_{\mathrm{CR=H,He}}\ \sum_{\mathrm{ISM=H,He}} n_{\mathrm{ISM}}(\mathbf{r})\int \mathrm{d}p'_{\mathrm{CR}}\,\beta_{\mathrm{CR}}\,c\frac{\mathrm{d}\sigma\left(p,p'_{\mathrm{CR}}\right)}{\mathrm{d}p}\,n_{\mathrm{CR}}\left(\mathbf{r},p'_{\mathrm{CR}}\right). \quad (5)$$

The density of hydrogen and helium gas is represented by $n_{\mathrm{ISM}}(\mathbf{r})$, and p'_{CR}, β_{CR} and $n_{\mathrm{CR}}(\mathbf{r}, p'_{\mathrm{CR}})$ are the momentum, the velocity and the density of the cosmic rays, while p is the momentum of the produced $^3\overline{\mathrm{He}}$. $\mathrm{d}\sigma(p, p'_{\mathrm{CR}})/\mathrm{d}p$ is the $^3\overline{\mathrm{He}}$ differential production cross section for the specific collision and includes primary $^3\overline{\mathrm{He}}$ as well as the products of $\bar{t}$ decays. The most abundant cosmic rays are protons and helium, thus this source function must be calculated for both species and summed up. In Ref. [51] all relevant types of collisions between protons and ^{4}He nuclei with projectile beam energies from 31 GeV to 12.5 TeV are considered, and the so-called spherical approximation is used in which antinucleons with a momentum difference smaller than p_0 are forming an antinucleus [51, 82]. The parameter p_0 depends on collision energy and is constrained by several accelerator-based measurements [1–17], including measurements at the LHC [83, 84]. The resulting injection spectra obtained from the collisions of cosmic rays with the ISM peak above 7 GeV/A [51].

In the case of $^3\overline{\mathrm{He}}$ nuclei produced from dark-matter annihilations, the source function depends on the thermally averaged inelastic cross section times velocity ($\langle\sigma v\rangle$), the density (ρ_{DM}) of the dark matter, the mass (m_χ) of the dark-matter particle and the resulting $^3\overline{\mathrm{He}}$ spectrum ($\mathrm{d}N/\mathrm{d}E_{\mathrm{kin}}$) [27]:

$$q(\mathbf{r}, E_{\mathrm{kin}}) = \frac{1}{2}\frac{\rho^2_{\mathrm{DM}}(\mathbf{r})}{m^2_\chi}\langle\sigma v\rangle\frac{\mathrm{d}N}{\mathrm{d}E_{\mathrm{kin}}}. \tag{6}$$

Here E_{kin} is the kinetic energy of the produced $^3\overline{\mathrm{He}}$ including those which are the products of $\bar{t}$ decays. The spectrum is calculated utilising the PYTHIA 8.156 event generator [85] and a coalescence model with a coalescence momentum $p_0 = 357$ MeV/c, as described in more detail in Ref. [27]. We set $\langle\sigma v\rangle = 2.6\times10^{-26}$ cm^{3}s^{-1} as provided in Ref. [28]. We implemented in GALPROP the Navarro–Frenk–White profile which is one of the most commonly used dark-matter density profiles:

$$\rho(r) = \frac{\rho_0}{\frac{r}{R_s}\left(1+\frac{r}{R_s}\right)^2}. \tag{7}$$

Here r is the distance to the galactic centre. ρ_0 is an overall normalization such that $\rho(r)$ is equal to the local density $\rho_\odot = 0.39$ GeV/cm^3 at $r = 8.5$ kpc and $R_s = 24.42$ kpc is a scale radius as given in Ref. [27]. In contrast to the spectra of $^3\overline{\mathrm{He}}$ from collisions of cosmic rays with the interstellar medium, the resulting spectrum for $^3\overline{\mathrm{He}}$ originating from dark-matter annihilation peaks at low kinetic energies around 0.1 GeV/A [27].

5.6 Discussion of uncertainties on $^3\overline{\mathrm{He}}$ cosmic-ray modelling

The results presented in this paper focus on the impact of the ALICE measurements for $\sigma_{\mathrm{inel}}(^3\overline{\mathrm{He}})$ on cosmic-ray $^3\overline{\mathrm{He}}$ flux and the corresponding transparency of the galaxy. To this purpose, we have considered two models of $^3\overline{\mathrm{He}}$ source described in the text and propagated only the uncertainty of the $\sigma_{\mathrm{inel}}(^3\overline{\mathrm{He}})$ measurement. This Section briefly discusses other possible uncertainties related to the $^3\overline{\mathrm{He}}$ cosmic-ray modelling.

As for the dark-matter source, it is apparent that a different dark-matter mass assumption changes the antinuclei flux profile near Earth [20, 27, 29]. The DM mass assumptions around $m_\chi \sim 100$ GeV are favoured by recent AMS-02 antiproton data [29]; for very different values of m_χ the $^3\overline{\mathrm{He}}$ flux and the corresponding transparency can be studied as described in this work. Variation of the dark-matter annihilation cross section $\langle\sigma v\rangle$ leads to a constant scaling of $^3\overline{\mathrm{He}}$ flux according to Eq. 6 and therefore to identical transparency values. While the Navarro–Frenk–White profile is used in this work to describe the distribution of dark matter in the galaxy, other profiles are also available such as Einasto [20], Burkert [86] or the isothermal one [87]. The effect of different DM profiles is degenerate with $\langle\sigma v\rangle$, and the overall impact on the antinuclei flux is minor [28, 56]. If the isothermal profile is employed instead of the Navarro–Frenk–White one, the obtained $^3\overline{\mathrm{He}}$ transparency is shifted up by $10-15\%$.

Although the coalescence-based models can successfully describe the antinuclei production, the model uncertainties are still relatively large, which leads to significant changes of the magnitude of antinuclei fluxes [20, 28, 56]. In general, as long as different coalescence models retain the shape of the produced antinuclei momentum spectrum, the resulting transparency is not affected. For example, the change of coalescence parameter p_0 leads to constant scaling of the antinuclei flux and identical transparency values.

The GALPROP parameters used in this work are tuned to reproduce the available experimental data on cosmic-ray nuclei (up to $Z = 28$). The obtained uncertainties on the nuclei fluxes of $\lesssim 10\%$ [40] are not considered in this work, since they result in a negligible change to the $^{3}\overline{\mathrm{He}}$ fluxes. An alternative set of propagation parameters has been obtained in Ref. [74] by considering a subsample of available cosmic-ray data. The comparison between the two sets is discussed in more details in Ref. [56]. The employment of these alternative parameters decreases the $^{3}\overline{\mathrm{He}}$ background flux by one order of magnitude at the lowest E_{kin} considered in this work and results in about 60% lower transparency. For dark-matter signal the corresponding flux is up to a factor 5 higher at the lowest E_{kin} with about 40% lower transparency. These differences in fluxes and transparencies are obtained before the solar modulation and become minor for $E_{\mathrm{kin}} \gtrsim 10$ GeV/A, both for dark-matter signal and for the background.

A The ALICE Collaboration

S. Acharya[142], D. Adamová[96], A. Adler[74], J. Adolfsson[81], G. Aglieri Rinella[34], M. Agnello[30], N. Agrawal[54], Z. Ahammed[142], S. Ahmad[16], S.U. Ahn[76], I. Ahuja[38], Z. Akbar[51], A. Akindinov[93], M. Al-Turany[108], S.N. Alam[16], D. Aleksandrov[89], B. Alessandro[59], H.M. Alfanda[7], R. Alfaro Molina[71], B. Ali[16], Y. Ali[14], A. Alici[25], N. Alizadehvandchali[125], A. Alkin[34], J. Alme[21], G. Alocco[55], T. Alt[68], I. Altsybeev[113], M.N. Anaam[7], C. Andrei[48], D. Andreou[91], A. Andronic[145], V. Anguelov[105], F. Antinori[57], P. Antonioli[54], C. Anuj[16], N. Apadula[80], L. Aphecetche[115], H. Appelshäuser[68], S. Arcelli[25], R. Arnaldi[59], I.C. Arsene[20], M. Arslandok[147], A. Augustinus[34], R. Averbeck[108], S. Aziz[78], M.D. Azmi[16], A. Badalà[56], Y.W. Baek[41], X. Bai[129,108], R. Bailhache[68], Y. Bailung[50], R. Bala[102], A. Balbino[30], A. Baldisseri[139], B. Balis[2], D. Banerjee[4], Z. Banoo[102], R. Barbera[26], L. Barioglio[106], M. Barlou[85], G.G. Barnaföldi[146], L.S. Barnby[95], V. Barret[136], C. Bartels[128], K. Barth[34], E. Bartsch[68], F. Baruffaldi[27], N. Bastid[136], S. Basu[81], G. Batigne[115], D. Battistini[106], B. Batyunya[75], D. Bauri[49], J.L. Bazo Alba[112], I.G. Bearden[90], C. Beattie[147], P. Becht[108], I. Belikov[138], A.D.C. Bell Hechavarria[145], F. Bellini[25], R. Bellwied[125], S. Belokurova[113], V. Belyaev[94], G. Bencedi[146,69], S. Beole[24], A. Bercuci[48], Y. Berdnikov[99], A. Berdnikova[105], L. Bergmann[105], M.G. Besoiu[67], L. Betev[34], P.P. Bhaduri[142], A. Bhasin[102], I.R. Bhat[102], M.A. Bhat[4], B. Bhattacharjee[42], P. Bhattacharya[22], L. Bianchi[24], N. Bianchi[52], J. Bielčík[37], J. Bielčíková[96], J. Biernat[118], A. Bilandzic[106], G. Biro[146], S. Biswas[4], J.T. Blair[119], D. Blau[89,82], M.B. Blidaru[108], C. Blume[68], G. Boca[28,58], F. Bock[97], A. Bogdanov[94], S. Boi[22], J. Bok[61], L. Boldizsár[146], A. Bolozdynya[94], M. Bombara[38], P.M. Bond[34], G. Bonomi[141,58], H. Borel[139], A. Borissov[82], H. Bossi[147], E. Botta[24], L. Bratrud[68], P. Braun-Munzinger[108], M. Bregant[121], M. Broz[37], G.E. Bruno[107,33], M.D. Buckland[23,128], D. Budnikov[109], H. Buesching[68], S. Bufalino[30], O. Bugnon[115], P. Buhler[114], Z. Buthelezi[72,132], J.B. Butt[14], A. Bylinkin[127], S.A. Bysiak[118], M. Cai[27,7], H. Caines[147], A. Caliva[108], E. Calvo Villar[112], J.M.M. Camacho[120], R.S. Camacho[45], P. Camerini[23], F.D.M. Canedo[121], M. Carabas[135], F. Carnesecchi[34,25], R. Caron[137,139], J. Castillo Castellanos[139], E.A.R. Casula[22], F. Catalano[30], C. Ceballos Sanchez[75], I. Chakaberia[80], P. Chakraborty[49], S. Chandra[142], S. Chapeland[34], M. Chartier[128], S. Chattopadhyay[142], S. Chattopadhyay[110], T.G. Chavez[45], T. Cheng[7], C. Cheshkov[137], B. Cheynis[137], V. Chibante Barroso[34], D.D. Chinellato[122], S. Cho[61], P. Chochula[34], P. Christakoglou[91], C.H. Christensen[90], P. Christiansen[81], T. Chujo[134], C. Cicalo[55], L. Cifarelli[25], F. Cindolo[54], M.R. Ciupek[108], G. Clai[II,54], J. Cleymans[I,124], F. Colamaria[53], J.S. Colburn[111], D. Colella[53,107,33], A. Collu[80], M. Colocci[25,34], M. Concas[III,59], G. Conesa Balbastre[79], Z. Conesa del Valle[78], G. Contin[23], J.G. Contreras[37], M.L. Coquet[139], T.M. Cormier[97], P. Cortese[31], M.R. Cosentino[123], F. Costa[34], S. Costanza[28,58], P. Crochet[136], R. Cruz-Torres[80], E. Cuautle[69], P. Cui[7], L. Cunqueiro[97], A. Dainese[57], M.C. Danisch[105], A. Danu[67], P. Das[87], P. Das[4], S. Das[4], S. Dash[49], A. De Caro[29], G. de Cataldo[53], L. De Cilladi[24], J. de Cuveland[39], A. De Falco[22], D. De Gruttola[29], N. De Marco[59], C. De Martin[23], S. De Pasquale[29], S. Deb[50], H.F. Degenhardt[121], K.R. Deja[143], R. Del Grande[106], L. Dello Stritto[29], W. Deng[7], P. Dhankher[19], D. Di Bari[33], A. Di Mauro[34], R.A. Diaz[8], T. Dietel[124], Y. Ding[137,7], R. Divià[34], D.U. Dixit[19], Ø. Djuvsland[21], U. Dmitrieva[63], J. Do[61], A. Dobrin[67], B. Dönigus[68], A.K. Dubey[142], A. Dubla[108,91], S. Dudi[101], P. Dupieux[136], M. Durkac[117], N. Dzalaiova[13], T.M. Eder[145], R.J. Ehlers[97], V.N. Eikeland[21], F. Eisenhut[68], D. Elia[53], B. Erazmus[115], F. Ercolessi[25], F. Erhardt[100], A. Erokhin[113], M.R. Ersdal[21], B. Espagnon[78], G. Eulisse[34], D. Evans[111], S. Evdokimov[92], L. Fabbietti[106], M. Faggin[27], J. Faivre[79], F. Fan[7], W. Fan[80], A. Fantoni[52], M. Fasel[97], P. Fecchio[30], A. Feliciello[59], G. Feofilov[113], A. Fernández Téllez[45], A. Ferrero[139], A. Ferretti[24], V.J.G. Feuillard[105], J. Figiel[118], V. Filova[37], D. Finogeev[63], F.M. Fionda[55], G. Fiorenza[34], F. Flor[125], A.N. Flores[119], S. Foertsch[72], S. Fokin[89], E. Fragiacomo[60], E. Frajna[146], A. Francisco[136], U. Fuchs[34], N. Funicello[29], C. Furget[79], A. Furs[63], J.J. Gaardhøje[90], M. Gagliardi[24], A.M. Gago[112], A. Gal[138], C.D. Galvan[120], P. Ganoti[85], C. Garabatos[108], J.R.A. Garcia[45], E. Garcia-Solis[10], K. Garg[115], C. Gargiulo[34], A. Garibli[88], K. Garner[145], P. Gasik[108], E.F. Gauger[119], A. Gautam[127], M.B. Gay Ducati[70], M. Germain[115], S.K. Ghosh[4], M. Giacalone[25], P. Gianotti[52], P. Giubellino[108,59], P. Giubilato[27], A.M.C. Glaenzer[139], P. Glässel[105], E. Glimos[131], D.J.Q. Goh[83], V. Gonzalez[144], L.H. González-Trueba[71], S. Gorbunov[39], M. Gorgon[2], L. Görlich[118], S. Gotovac[35], V. Grabski[71], L.K. Graczykowski[143], L. Greiner[80], A. Grelli[62], C. Grigoras[34], V. Grigoriev[94], S. Grigoryan[75,1], F. Grosa[34,59], J.F. Grosse-Oetringhaus[34], R. Grosso[108], D. Grund[37], G.G. Guardiano[122], R. Guernane[79], M. Guilbaud[115], K. Gulbrandsen[90], T. Gunji[133], W. Guo[7], A. Gupta[102], R. Gupta[102], S.P. Guzman[45], L. Gyulai[146], M.K. Habib[108], C. Hadjidakis[78], H. Hamagaki[83], M. Hamid[7], R. Hannigan[119], M.R. Haque[143], A. Harlenderova[108], J.W. Harris[147], A. Harton[10], J.A. Hasenbichler[34], H. Hassan[97], D. Hatzifotiadou[54], P. Hauer[43], L.B. Havener[147], S.T. Heckel[106], E. Hellbär[108], H. Helstrup[36], T. Herman[37], G. Herrera Corral[9], F. Herrmann[145], K.F. Hetland[36], H. Hillemanns[34], C. Hills[128], B. Hippolyte[138], B. Hofman[62], B. Hohlweger[91], J. Honermann[145], G.H. Hong[148], D. Horak[37], S. Hornung[108], A. Horzyk[2], R. Hosokawa[15], Y. Hou[7], P. Hristov[34], C. Hughes[131], P. Huhn[68], L.M. Huhta[126], C.V. Hulse[78], T.J. Humanic[98], H. Hushnud[110], L.A. Husova[145], A. Hutson[125], J.P. Iddon[34,128], R. Ilkaev[109], H. Ilyas[14],

M. Inaba[134], G.M. Innocenti[34], M. Ippolitov[89], A. Isakov[96], T. Isidori[127], M.S. Islam[110], M. Ivanov[108], V. Ivanov[99], V. Izucheev[92], M. Jablonski[2], B. Jacak[80], N. Jacazio[34], P.M. Jacobs[80], S. Jadlovska[117], J. Jadlovsky[117], S. Jaelani[62], C. Jahnke[122,121], M.J. Jakubowska[143], A. Jalotra[102], M.A. Janik[143], T. Janson[74], M. Jercic[100], O. Jevons[111], A.A.P. Jimenez[69], F. Jonas[97,145], P.G. Jones[111], J.M. Jowett [34,108], J. Jung[68], M. Jung[68], A. Junique[34], A. Jusko[111], M.J. Kabus[143], J. Kaewjai[116], P. Kalinak[64], A.S. Kalteyer[108], A. Kalweit[34], V. Kaplin[94], A. Karasu Uysal[77], D. Karatovic[100], O. Karavichev[63], T. Karavicheva[63], P. Karczmarczyk[143], E. Karpechev[63], V. Kashyap[87], A. Kazantsev[89], U. Kebschull[74], R. Keidel[47], D.L.D. Keijdener[62], M. Keil[34], B. Ketzer[43], A.M. Khan[7], S. Khan[16], A. Khanzadeev[99], Y. Kharlov[92,82], A. Khatun[16], A. Khuntia[118], B. Kileng[36], B. Kim[17,61], C. Kim[17], D.J. Kim[126], E.J. Kim[73], J. Kim[148], J.S. Kim[41], J. Kim[105], J. Kim[73], M. Kim[105], S. Kim[18], T. Kim[148], S. Kirsch[68], I. Kisel[39], S. Kiselev[93], A. Kisiel[143], J.P. Kitowski[2], J.L. Klay[6], J. Klein[34], S. Klein[80], C. Klein-Bösing[145], M. Kleiner[68], T. Klemenz[106], A. Kluge[34], A.G. Knospe[125], C. Kobdaj[116], T. Kollegger[108], A. Kondratyev[75], N. Kondratyeva[94], E. Kondratyuk[92], J. Konig[68], S.A. Konigstorfer[106], P.J. Konopka[34], G. Kornakov[143], S.D. Koryciak[2], A. Kotliarov[96], O. Kovalenko[86], V. Kovalenko[113], M. Kowalski[118], I. Králik[64], A. Kravčáková[38], L. Kreis[108], M. Krivda[111,64], F. Krizek[96], K. Krizkova Gajdosova[37], M. Kroesen[105], M. Krüger[68], D.M. Krupova[37], E. Kryshen[99], M. Krzewicki[39], V. Kučera[34], C. Kuhn[138], P.G. Kuijer[91], T. Kumaoka[134], D. Kumar[142], L. Kumar[101], N. Kumar[101], S. Kundu[34], P. Kurashvili[86], A. Kurepin[63], A.B. Kurepin[63], A. Kuryakin[109], S. Kushpil[96], J. Kvapil[111], M.J. Kweon[61], J.Y. Kwon[61], Y. Kwon[148], S.L. La Pointe[39], P. La Rocca[26], Y.S. Lai[80], A. Lakrathok[116], M. Lamanna[34], R. Langoy[130], P. Larionov[34,52], E. Laudi[34], L. Lautner[34,106], R. Lavicka[114,37], T. Lazareva[113], R. Lea[141,23,58], J. Lehrbach[39], R.C. Lemmon[95], I. León Monzón[120], M.M. Lesch[106], E.D. Lesser[19], M. Lettrich[34,106], P. Lévai[146], X. Li[11], X.L. Li[7], J. Lien[130], R. Lietava[111], B. Lim[17], S.H. Lim[17], V. Lindenstruth[39], A. Lindner[48], C. Lippmann[108], A. Liu[19], D.H. Liu[7], J. Liu[128], I.M. Lofnes[21], V. Loginov[94], C. Loizides[97], P. Loncar[35], J.A. Lopez[105], X. Lopez[136], E. López Torres[8], J.R. Luhder[145], M. Lunardon[27], G. Luparello[60], Y.G. Ma[40], A. Maevskaya[63], M. Mager[34], T. Mahmoud[43], A. Maire[138], M. Malaev[99], N.M. Malik[102], Q.W. Malik[20], S.K. Malik[102], L. Malinina[IV,75], D. Mal'Kevich[93], D. Mallick[87], N. Mallick[50], G. Mandaglio[32,56], V. Manko[89], F. Manso[136], V. Manzari[53], Y. Mao[7], G.V. Margagliotti[23], A. Margotti[54], A. Marín[108], C. Markert[119], M. Marquard[68], N.A. Martin[105], P. Martinengo[34], J.L. Martinez[125], M.I. Martínez[45], G. Martínez García[115], S. Masciocchi[108], M. Masera[24], A. Masoni[55], L. Massacrier[78], A. Mastroserio[140,53], A.M. Mathis[106], O. Matonoha[81], P.F.T. Matuoka[121], A. Matyja[118], C. Mayer[118], A.L. Mazuecos[34], F. Mazzaschi[24], M. Mazzilli[34], J.E. Mdhluli[132], A.F. Mechler[68], Y. Melikyan[63], A. Menchaca-Rocha[71], E. Meninno[114,29], A.S. Menon[125], M. Meres[13], S. Mhlanga[124,72], Y. Miake[134], L. Micheletti[59], L.C. Migliorin[137], D.L. Mihaylov[106], K. Mikhaylov[75,93], A.N. Mishra[146], D. Miśkowiec[108], A. Modak[4], A.P. Mohanty[62], B. Mohanty[87], M. Mohisin Khan[V,16], M.A. Molander[44], Z. Moravcova[90], C. Mordasini[106], D.A. Moreira De Godoy[145], I. Morozov[63], A. Morsch[34], T. Mrnjavac[34], V. Muccifora[52], E. Mudnic[35], D. Mühlheim[145], S. Muhuri[142], J.D. Mulligan[80], A. Mulliri[22], M.G. Munhoz[121], R.H. Munzer[68], H. Murakami[133], S. Murray[124], L. Musa[34], J. Musinsky[64], J.W. Myrcha[143], B. Naik[132], R. Nair[86], B.K. Nandi[49], R. Nania[54], E. Nappi[53], A.F. Nassirpour[81], A. Nath[105], C. Nattrass[131], A. Neagu[20], A. Negru[135], L. Nellen[69], S.V. Nesbo[36], G. Neskovic[39], D. Nesterov[113], B.S. Nielsen[90], E.G. Nielsen[90], S. Nikolaev[89], S. Nikulin[89], V. Nikulin[99], F. Noferini[54], S. Noh[12], P. Nomokonov[75], J. Norman[128], N. Novitzky[134], P. Nowakowski[143], A. Nyanin[89], J. Nystrand[21], M. Ogino[83], A. Ohlson[81], V.A. Okorokov[94], J. Oleniacz[143], A.C. Oliveira Da Silva[131], M.H. Oliver[147], A. Onnerstad[126], C. Oppedisano[59], A. Ortiz Velasquez[69], T. Osako[46], A. Oskarsson[81], J. Otwinowski[118], M. Oya[46], K. Oyama[83], Y. Pachmayer[105], S. Padhan[49], D. Pagano[141,58], G. Paić[69], A. Palasciano[53], S. Panebianco[139], J. Park[61], J.E. Parkkila[126], S.P. Pathak[125], R.N. Patra[102,34], B. Paul[22], H. Pei[7], T. Peitzmann[62], X. Peng[7], L.G. Pereira[70], H. Pereira Da Costa[139], D. Peresunko[89,82], G.M. Perez[8], S. Perrin[139], Y. Pestov[5], V. Petráček[37], M. Petrovici[48], R.P. Pezzi[115,70], S. Piano[60], M. Pikna[13], P. Pillot[115], O. Pinazza[54,34], L. Pinsky[125], C. Pinto[26], S. Pisano[52], M. Płoskoń[80], M. Planinic[100], F. Pliquett[68], M.G. Poghosyan[97], B. Polichtchouk[92], S. Politano[30], N. Poljak[100], A. Pop[48], S. Porteboeuf-Houssais[136], J. Porter[80], V. Pozdniakov[75], S.K. Prasad[4], R. Preghenella[54], F. Prino[59], C.A. Pruneau[144], I. Pshenichnov[63], M. Puccio[34], S. Qiu[91], L. Quaglia[24], R.E. Quishpe[125], S. Ragoni[111], A. Rakotozafindrabe[139], L. Ramello[31], F. Rami[138], S.A.R. Ramirez[45], T.A. Rancien[79], R. Raniwala[103], S. Raniwala[103], S.S. Räsänen[44], R. Rath[50], I. Ravasenga[91], K.F. Read[97,131], A.R. Redelbach[39], K. Redlich[VI,86], A. Rehman[21], P. Reichelt[68], F. Reidt[34], H.A. Reme-ness[36], Z. Rescakova[38], K. Reygers[105], A. Riabov[99], V. Riabov[99], T. Richert[81], M. Richter[20], W. Riegler[34], F. Riggi[26], C. Ristea[67], M. Rodríguez Cahuantzi[45], K. Røed[20], R. Rogalev[92], E. Rogochaya[75], T.S. Rogoschinski[68], D. Rohr[34], D. Röhrich[21], P.F. Rojas[45], S. Rojas Torres[37], P.S. Rokita[143], F. Ronchetti[52], A. Rosano[32,56], E.D. Rosas[69], A. Rossi[57], A. Roy[50], P. Roy[110], S. Roy[49], N. Rubini[25], O.V. Rueda[81], D. Ruggiano[143], R. Rui[23], B. Rumyantsev[75], P.G. Russek[2], R. Russo[91], A. Rustamov[88], E. Ryabinkin[89], Y. Ryabov[99], A. Rybicki[118], H. Rytkonen[126], W. Rzesa[143], O.A.M. Saarimaki[44], R. Sadek[115], S. Sadovsky[92], J. Saetre[21], K. Šafařík[37], S.K. Saha[142], S. Saha[87], B. Sahoo[49], P. Sahoo[49], R. Sahoo[50], S. Sahoo[65], D. Sahu[50], P.K. Sahu[65], J. Saini[142], S. Sakai[134], M.P. Salvan[108], S. Sambyal[102], T.B. Saramela[121], D. Sarkar[144], N. Sarkar[142], P. Sarma[42], V.M. Sarti[106], M.H.P. Sas[147], J. Schambach[97], H.S. Scheid[68], C. Schiaua[48], R. Schicker[105], A. Schmah[105], C. Schmidt[108], H.R. Schmidt[104], M.O. Schmidt[34,105], M. Schmidt[104], N.V. Schmidt[97,68], A.R. Schmier[131], R. Schotter[138], J. Schukraft[34], K. Schwarz[108], K. Schweda[108], G. Scioli[25], E. Scomparin[59], J.E. Seger[15], Y. Sekiguchi[133], D. Sekihata[133], I. Selyuzhenkov[108,94], S. Senyukov[138], J.J. Seo[61], D. Serebryakov[63], L. Šerkšnytė[106], A. Sevcenco[67], T.J. Shaba[72], A. Shabanov[63], A. Shabetai[115], R. Shahoyan[34], W. Shaikh[110], A. Shangaraev[92], A. Sharma[101], H. Sharma[118], M. Sharma[102], N. Sharma[101], S. Sharma[102], U. Sharma[102], A. Shatat[78], O. Sheibani[125], K. Shigaki[46], M. Shimomura[84], S. Shirinkin[93], Q. Shou[40], Y. Sibiriak[89], S. Siddhanta[55], T. Siemiarczuk[86], T.F. Silva[121], D. Silvermyr[81], T. Simantathammakul[116], G. Simonetti[34], B. Singh[106], R. Singh[87], R. Singh[102], R. Singh[50], V.K. Singh[142], V. Singhal[142], T. Sinha[110], B. Sitar[13], M. Sitta[31], T.B. Skaali[20], G. Skorodumovs[105], M. Slupecki[44], N. Smirnov[147], R.J.M. Snellings[62], C. Soncco[112], J. Song[125], A. Songmoolnak[116], F. Soramel[27], S. Sorensen[131], I. Sputowska[118], J. Stachel[105], I. Stan[67], P.J. Steffanic[131], S.F. Stiefelmaier[105], D. Stocco[115], I. Storehaug[20], M.M. Storetvedt[36], P. Stratmann[145], S. Strazzi[25], C.P. Stylianidis[91], A.A.P. Suaide[121], C. Suire[78], M. Sukhanov[63], M. Suljic[34], R. Sultanov[93], V. Sumberia[102], S. Sumowidagdo[51], S. Swain[65], A. Szabo[13], I. Szarka[13], U. Tabassam[14], S.F. Taghavi[106], G. Taillepied[108,136], J. Takahashi[122], G.J. Tambave[21], S. Tang[136,7], Z. Tang[129], J.D. Tapia Takaki[VII,127], N. Tapus[135], M.G. Tarzila[48], A. Tauro[34], G. Tejeda Muñoz[45], A. Telesca[34], L. Terlizzi[24], C. Terrevoli[125], G. Tersimonov[3], S. Thakur[142], D. Thomas[119], R. Tieulent[137], A. Tikhonov[63], A.R. Timmins[125], M. Tkacik[117], A. Toia[68], N. Topilskaya[63], M. Toppi[52], F. Torales-Acosta[19], T. Tork[78], A.G. Torres Ramos[33], A. Trifiró[32,56], A.S. Triolo[32], S. Tripathy[54,69], T. Tripathy[49], S. Trogolo[34,27], V. Trubnikov[3], W.H. Trzaska[126], T.P. Trzcinski[143], A. Tumkin[109], R. Turrisi[57], T.S. Tveter[20], K. Ullaland[21], A. Uras[137], M. Urioni[58,141], G.L. Usai[22], M. Vala[38], N. Valle[28], S. Vallero[59], L.V.R. van Doremalen[62], M. van Leeuwen[91], P. Vande Vyvre[34], D. Varga[146], Z. Varga[146], M. Varga-Kofarago[146], M. Vasileiou[85], A. Vasiliev[89], O. Vázquez Doce[52,106], V. Vechernin[113], A. Velure[21], E. Vercellin[24], S. Vergara Limón[45], L. Vermunt[62], R. Vértesi[146], M. Verweij[62], L. Vickovic[35], Z. Vilakazi[132], O. Villalobos Baillie[111], G. Vino[53], A. Vinogradov[89], T. Virgili[29], V. Vislavicius[90], A. Vodopyanov[75], B. Volkel[34,105], M.A. Völkl[105], K. Voloshin[93], S.A. Voloshin[144], G. Volpe[33], B. von Haller[34], I. Vorobyev[106], N. Vozniuk[63], J. Vrláková[38], B. Wagner[21], C. Wang[40], D. Wang[40], M. Weber[114], R.J.G.V. Weelden[91], A. Wegrzynek[34], S.C. Wenzel[34], J.P. Wessels[145], S.L. Weyhmiller[147], J. Wiechula[68], J. Wikne[20], G. Wilk[86], J. Wilkinson[108], G.A. Willems[145], B. Windelband[105], M. Winn[139], W.E. Witt[131], J.R. Wright[119], W. Wu[40], Y. Wu[129], R. Xu[7], A.K. Yadav[142], S. Yalcin[77], Y. Yamaguchi[46], K. Yamakawa[46], S. Yang[21], S. Yano[46], Z. Yin[7], I.-K. Yoo[17], J.H. Yoon[61], S. Yuan[21], A. Yuncu[105], V. Zaccolo[23], C. Zampolli[34], H.J.C. Zanoli[62], F. Zanone[105], N. Zardoshti[34], A. Zarochentsev[113], P. Závada[66], N. Zaviyalov[109], M. Zhalov[99], B. Zhang[7], S. Zhang[40], X. Zhang[7], Y. Zhang[129], V. Zherebchevskii[113], Y. Zhi[11], N. Zhigareva[93], D. Zhou[7], Y. Zhou[90], J. Zhu[108,7], Y. Zhu[7], G. Zinovjev[I,3], N. Zurlo[141,58]

Affiliation Notes

[I] Deceased
[II] Also at: Italian National Agency for New Technologies, Energy and Sustainable Economic Development (ENEA), Bologna, Italy
[III] Also at: Dipartimento DET del Politecnico di Torino, Turin, Italy
[IV] Also at: M.V. Lomonosov Moscow State University, D.V. Skobeltsyn Institute of Nuclear, Physics, Moscow, Russia
[V] Also at: Department of Applied Physics, Aligarh Muslim University, Aligarh, India
[VI] Also at: Institute of Theoretical Physics, University of Wroclaw, Poland
[VII] Also at: University of Kansas, Lawrence, Kansas, United States

Collaboration Institutes

[1] A.I. Alikhanyan National Science Laboratory (Yerevan Physics Institute) Foundation, Yerevan, Armenia
[2] AGH University of Science and Technology, Cracow, Poland
[3] Bogolyubov Institute for Theoretical Physics, National Academy of Sciences of Ukraine, Kiev, Ukraine
[4] Bose Institute, Department of Physics and Centre for Astroparticle Physics and Space Science (CAPSS), Kolkata, India
[5] Budker Institute for Nuclear Physics, Novosibirsk, Russia
[6] California Polytechnic State University, San Luis Obispo, California, United States

[7] Central China Normal University, Wuhan, China
[8] Centro de Aplicaciones Tecnológicas y Desarrollo Nuclear (CEADEN), Havana, Cuba
[9] Centro de Investigación y de Estudios Avanzados (CINVESTAV), Mexico City and Mérida, Mexico
[10] Chicago State University, Chicago, Illinois, United States
[11] China Institute of Atomic Energy, Beijing, China
[12] Chungbuk National University, Cheongju, Republic of Korea
[13] Comenius University Bratislava, Faculty of Mathematics, Physics and Informatics, Bratislava, Slovakia
[14] COMSATS University Islamabad, Islamabad, Pakistan
[15] Creighton University, Omaha, Nebraska, United States
[16] Department of Physics, Aligarh Muslim University, Aligarh, India
[17] Department of Physics, Pusan National University, Pusan, Republic of Korea
[18] Department of Physics, Sejong University, Seoul, Republic of Korea
[19] Department of Physics, University of California, Berkeley, California, United States
[20] Department of Physics, University of Oslo, Oslo, Norway
[21] Department of Physics and Technology, University of Bergen, Bergen, Norway
[22] Dipartimento di Fisica dell'Università and Sezione INFN, Cagliari, Italy
[23] Dipartimento di Fisica dell'Università and Sezione INFN, Trieste, Italy
[24] Dipartimento di Fisica dell'Università and Sezione INFN, Turin, Italy
[25] Dipartimento di Fisica e Astronomia dell'Università and Sezione INFN, Bologna, Italy
[26] Dipartimento di Fisica e Astronomia dell'Università and Sezione INFN, Catania, Italy
[27] Dipartimento di Fisica e Astronomia dell'Università and Sezione INFN, Padova, Italy
[28] Dipartimento di Fisica e Nucleare e Teorica, Università di Pavia, Pavia, Italy
[29] Dipartimento di Fisica 'E.R. Caianiello' dell'Università and Gruppo Collegato INFN, Salerno, Italy
[30] Dipartimento DISAT del Politecnico and Sezione INFN, Turin, Italy
[31] Dipartimento di Scienze e Innovazione Tecnologica dell'Università del Piemonte Orientale and INFN Sezione di Torino, Alessandria, Italy
[32] Dipartimento di Scienze MIFT, Università di Messina, Messina, Italy
[33] Dipartimento Interateneo di Fisica 'M. Merlin' and Sezione INFN, Bari, Italy
[34] European Organization for Nuclear Research (CERN), Geneva, Switzerland
[35] Faculty of Electrical Engineering, Mechanical Engineering and Naval Architecture, University of Split, Split, Croatia
[36] Faculty of Engineering and Science, Western Norway University of Applied Sciences, Bergen, Norway
[37] Faculty of Nuclear Sciences and Physical Engineering, Czech Technical University in Prague, Prague, Czech Republic
[38] Faculty of Science, P.J. Šafárik University, Košice, Slovakia
[39] Frankfurt Institute for Advanced Studies, Johann Wolfgang Goethe-Universität Frankfurt, Frankfurt, Germany
[40] Fudan University, Shanghai, China
[41] Gangneung-Wonju National University, Gangneung, Republic of Korea
[42] Gauhati University, Department of Physics, Guwahati, India
[43] Helmholtz-Institut für Strahlen- und Kernphysik, Rheinische Friedrich-Wilhelms-Universität Bonn, Bonn, Germany
[44] Helsinki Institute of Physics (HIP), Helsinki, Finland
[45] High Energy Physics Group, Universidad Autónoma de Puebla, Puebla, Mexico
[46] Hiroshima University, Hiroshima, Japan
[47] Hochschule Worms, Zentrum für Technologietransfer und Telekommunikation (ZTT), Worms, Germany
[48] Horia Hulubei National Institute of Physics and Nuclear Engineering, Bucharest, Romania
[49] Indian Institute of Technology Bombay (IIT), Mumbai, India
[50] Indian Institute of Technology Indore, Indore, India
[51] Indonesian Institute of Sciences, Jakarta, Indonesia
[52] INFN, Laboratori Nazionali di Frascati, Frascati, Italy
[53] INFN, Sezione di Bari, Bari, Italy
[54] INFN, Sezione di Bologna, Bologna, Italy
[55] INFN, Sezione di Cagliari, Cagliari, Italy
[56] INFN, Sezione di Catania, Catania, Italy
[57] INFN, Sezione di Padova, Padova, Italy
[58] INFN, Sezione di Pavia, Pavia, Italy

[59] INFN, Sezione di Torino, Turin, Italy
[60] INFN, Sezione di Trieste, Trieste, Italy
[61] Inha University, Incheon, Republic of Korea
[62] Institute for Gravitational and Subatomic Physics (GRASP), Utrecht University/Nikhef, Utrecht, Netherlands
[63] Institute for Nuclear Research, Academy of Sciences, Moscow, Russia
[64] Institute of Experimental Physics, Slovak Academy of Sciences, Košice, Slovakia
[65] Institute of Physics, Homi Bhabha National Institute, Bhubaneswar, India
[66] Institute of Physics of the Czech Academy of Sciences, Prague, Czech Republic
[67] Institute of Space Science (ISS), Bucharest, Romania
[68] Institut für Kernphysik, Johann Wolfgang Goethe-Universität Frankfurt, Frankfurt, Germany
[69] Instituto de Ciencias Nucleares, Universidad Nacional Autónoma de México, Mexico City, Mexico
[70] Instituto de Física, Universidade Federal do Rio Grande do Sul (UFRGS), Porto Alegre, Brazil
[71] Instituto de Física, Universidad Nacional Autónoma de México, Mexico City, Mexico
[72] iThemba LABS, National Research Foundation, Somerset West, South Africa
[73] Jeonbuk National University, Jeonju, Republic of Korea
[74] Johann-Wolfgang-Goethe Universität Frankfurt Institut für Informatik, Fachbereich Informatik und Mathematik, Frankfurt, Germany
[75] Joint Institute for Nuclear Research (JINR), Dubna, Russia
[76] Korea Institute of Science and Technology Information, Daejeon, Republic of Korea
[77] KTO Karatay University, Konya, Turkey
[78] Laboratoire de Physique des 2 Infinis, Irène Joliot-Curie, Orsay, France
[79] Laboratoire de Physique Subatomique et de Cosmologie, Université Grenoble-Alpes, CNRS-IN2P3, Grenoble, France
[80] Lawrence Berkeley National Laboratory, Berkeley, California, United States
[81] Lund University Department of Physics, Division of Particle Physics, Lund, Sweden
[82] Moscow Institute for Physics and Technology, Moscow, Russia
[83] Nagasaki Institute of Applied Science, Nagasaki, Japan
[84] Nara Women's University (NWU), Nara, Japan
[85] National and Kapodistrian University of Athens, School of Science, Department of Physics , Athens, Greece
[86] National Centre for Nuclear Research, Warsaw, Poland
[87] National Institute of Science Education and Research, Homi Bhabha National Institute, Jatni, India
[88] National Nuclear Research Center, Baku, Azerbaijan
[89] National Research Centre Kurchatov Institute, Moscow, Russia
[90] Niels Bohr Institute, University of Copenhagen, Copenhagen, Denmark
[91] Nikhef, National institute for subatomic physics, Amsterdam, Netherlands
[92] NRC Kurchatov Institute IHEP, Protvino, Russia
[93] NRC «Kurchatov»Institute - ITEP, Moscow, Russia
[94] NRNU Moscow Engineering Physics Institute, Moscow, Russia
[95] Nuclear Physics Group, STFC Daresbury Laboratory, Daresbury, United Kingdom
[96] Nuclear Physics Institute of the Czech Academy of Sciences, Řež u Prahy, Czech Republic
[97] Oak Ridge National Laboratory, Oak Ridge, Tennessee, United States
[98] Ohio State University, Columbus, Ohio, United States
[99] Petersburg Nuclear Physics Institute, Gatchina, Russia
[100] Physics department, Faculty of science, University of Zagreb, Zagreb, Croatia
[101] Physics Department, Panjab University, Chandigarh, India
[102] Physics Department, University of Jammu, Jammu, India
[103] Physics Department, University of Rajasthan, Jaipur, India
[104] Physikalisches Institut, Eberhard-Karls-Universität Tübingen, Tübingen, Germany
[105] Physikalisches Institut, Ruprecht-Karls-Universität Heidelberg, Heidelberg, Germany
[106] Physik Department, Technische Universität München, Munich, Germany
[107] Politecnico di Bari and Sezione INFN, Bari, Italy
[108] Research Division and ExtreMe Matter Institute EMMI, GSI Helmholtzzentrum für Schwerionenforschung GmbH, Darmstadt, Germany
[109] Russian Federal Nuclear Center (VNIIEF), Sarov, Russia
[110] Saha Institute of Nuclear Physics, Homi Bhabha National Institute, Kolkata, India
[111] School of Physics and Astronomy, University of Birmingham, Birmingham, United Kingdom

[112] Sección Física, Departamento de Ciencias, Pontificia Universidad Católica del Perú, Lima, Peru
[113] St. Petersburg State University, St. Petersburg, Russia
[114] Stefan Meyer Institut für Subatomare Physik (SMI), Vienna, Austria
[115] SUBATECH, IMT Atlantique, Université de Nantes, CNRS-IN2P3, Nantes, France
[116] Suranaree University of Technology, Nakhon Ratchasima, Thailand
[117] Technical University of Košice, Košice, Slovakia
[118] The Henryk Niewodniczanski Institute of Nuclear Physics, Polish Academy of Sciences, Cracow, Poland
[119] The University of Texas at Austin, Austin, Texas, United States
[120] Universidad Autónoma de Sinaloa, Culiacán, Mexico
[121] Universidade de São Paulo (USP), São Paulo, Brazil
[122] Universidade Estadual de Campinas (UNICAMP), Campinas, Brazil
[123] Universidade Federal do ABC, Santo Andre, Brazil
[124] University of Cape Town, Cape Town, South Africa
[125] University of Houston, Houston, Texas, United States
[126] University of Jyväskylä, Jyväskylä, Finland
[127] University of Kansas, Lawrence, Kansas, United States
[128] University of Liverpool, Liverpool, United Kingdom
[129] University of Science and Technology of China, Hefei, China
[130] University of South-Eastern Norway, Tonsberg, Norway
[131] University of Tennessee, Knoxville, Tennessee, United States
[132] University of the Witwatersrand, Johannesburg, South Africa
[133] University of Tokyo, Tokyo, Japan
[134] University of Tsukuba, Tsukuba, Japan
[135] University Politehnica of Bucharest, Bucharest, Romania
[136] Université Clermont Auvergne, CNRS/IN2P3, LPC, Clermont-Ferrand, France
[137] Université de Lyon, CNRS/IN2P3, Institut de Physique des 2 Infinis de Lyon, Lyon, France
[138] Université de Strasbourg, CNRS, IPHC UMR 7178, F-67000 Strasbourg, France, Strasbourg, France
[139] Université Paris-Saclay Centre d'Etudes de Saclay (CEA), IRFU, Départment de Physique Nucléaire (DPhN), Saclay, France
[140] Università degli Studi di Foggia, Foggia, Italy
[141] Università di Brescia, Brescia, Italy
[142] Variable Energy Cyclotron Centre, Homi Bhabha National Institute, Kolkata, India
[143] Warsaw University of Technology, Warsaw, Poland
[144] Wayne State University, Detroit, Michigan, United States
[145] Westfälische Wilhelms-Universität Münster, Institut für Kernphysik, Münster, Germany
[146] Wigner Research Centre for Physics, Budapest, Hungary
[147] Yale University, New Haven, Connecticut, United States
[148] Yonsei University, Seoul, Republic of Korea